Geochimica et Cosmochimica Acta 369 (2024) 111–125

Contents lists available at ScienceDirect

Geochimica et Cosmochimica Acta

journal homepage: www.elsevier.com/locate/gca

BrGDGT lipids in cold regions reflect summer soil temperature and seasonal soil water chemistry

Jonathan H. Raberg [a,*], Sarah E. Crump [b,1], Greg de Wet [c], David J. Harning [a], Gifford H. Miller [a,d], Áslaug Geirsdóttir [e], Julio Sepúlveda [a,d]

[a] Institute of Arctic and Alpine Research, University of Colorado Boulder, USA
[b] Department of Geology and Geophysics, University of Utah, Salt Lake City, UT, USA
[c] Department of Geosciences, Smith College, Northampton, MA, USA
[d] Department of Geological Sciences, University of Colorado Boulder, USA
[e] Faculty of Earth Sciences, University of Iceland, Reykjavík, Iceland

ARTICLE INFO

Associate editor: Xiaojuan Feng

Keywords:
brGDGT
Paleoclimate
Biomarker
Soil temperature

ABSTRACT

The distribution of brGDGT lipids produced by soil bacteria has been used to reconstruct temperatures in marine and terrestrial settings as far back as the Cretaceous period. However, modern calibrations of this proxy have primarily relied on air rather than in situ soil temperatures, which can differ by more than 10 °C. Furthermore, the influence of other parameters such as temperature seasonality and soil chemistry on brGDGT lipids is not fully understood. We measured brGDGT distributions, in situ soil temperatures, pH, soil water content, and electrical conductivity on soils from the Eastern Canadian Arctic and Iceland. We compiled our results with those of published soil brGDGT studies that also provide in situ soil temperatures and ancilliary measurements and generated global temperature and pH calibrations from the resulting dataset. Soil temperatures outperformed air temperatures in these calibrations, with mean summer soil temperature providing the highest-performing fit among the 10 tested soil temperature parameters. When applied to a loess/paleosol sequence from the Chinese Loess Plateau, these new calibrations produced paleotemperature and paleo-pH histories consistent with the results of previous studies, encouraging the application of our new calibrations on a broader scale. We also detected 7-methyl and IIIa'' brGDGT isomers in our Eastern Canadian Arctic and Iceland soils, which have been shown in lakes to relate to salinity and anoxia, respectively. While neither correlated with bulk soil properties such as conductivity, soil water content, or pH, these brGDGT isomers did correlate with seasonality and winter soil temperature. We hypothesize that these compounds are generated in winter by bacteria in habitable niches of more saline, sometimes anoxic liquid water in the otherwise frozen soil matrix. Finally, we report the presence of overly branched GDGTs with m/z = 1064 and suggest that these heptamethylated tetraethers should be investigated as a potential tool for improving brGDGT calibrations. Overall, our results expand our understanding of the seasonality of brGDGT production, especially at high latitudes, and provide in situ soil temperature and pH calibrations for global use.

1. Introduction

As temperatures rise globally due to anthropogenic climate change (IPCC, 2022), our ability to constrain future climate regimes can be greatly aided by reconstructing those of the past (Tierney et al., 2020). Lipid biomarkers are a useful tool in such pursuits due to their high preservation potential and abundance in nature (e.g., Sachs et al., 2013; Inglis et al., 2022). Of these, branched glycerol dialkyl glycerol tetraethers (brGDGTs) have shown promise as a quantitative terrestrial paleotemperature proxy. The structure of these lipids, which are bacterial in origin (Weijers et al., 2006), has been shown in environmental (e.g., Weijers et al., 2007b; Tierney et al., 2010; Zhao et al., 2020; Raberg et al., 2022b), laboratory (Chen et al., 2022; Halamka et al., 2022), and simulation (Naafs et al., 2021) studies to encode temperature through the variable number of methylations on their alkyl backbone. This relationship has been quantified with increasing precision in an

* Corresponding author.
E-mail address: jonathan.raberg@colorado.edu (J.H. Raberg).
[1] Deceased 18 November 2022.

https://doi.org/10.1016/j.gca.2024.01.034
Received 18 July 2023; Accepted 30 January 2024
Available online 7 February 2024

ever-growing number of samples through statistical and methodological advancements over the past ~15 years (e.g., in soils: Peterse et al., 2012; De Jonge et al., 2014; Naafs et al., 2017; Dearing Crampton-Flood et al., 2020; Dugerdil et al., 2021; Véquaud et al., 2022; Zhao et al., 2022). Such calibration efforts have paved the way for terrestrial paleotemperature reconstructions from soil brGDGTs in near-shore marine sediments (e.g., Weijers et al., 2007a; Weijers et al., 2007c; Pancost et al., 2013; Kemp et al., 2014; Tibbett et al., 2022) and terrestrial sequences, including loess, paleosol, and bone (e.g., Schreuder et al., 2016; Dillon et al., 2018; Super et al., 2018; Lu et al., 2022; Fuchs et al., 2022). Correlations between brGDGTs and soil pH (e.g., Peterse et al., 2012; De Jonge et al., 2014) further expand the utility of these lipids for paleoenvironmental reconstructions (e.g., Peterse et al., 2014; Sun et al., 2019). Still, uncertainties remain that complicate the use of soil-derived brGDGTs as an accurate paleoenvironmental proxy.

A key challenge in the development of brGDGT calibrations is determining specifically which temperatures are most closely reflected in the lipids' distributions. Traditionally, air temperatures have been used for brGDGT soil calibrations, due in part to their wide availability from metereological stations. However, air temperatures are themselves only a proxy for the soil temperatures experienced by a brGDGT-producing bacterium and are thus not ideal for calibration efforts (Molnar, 2022). In fact, air and soil temperatures can be offset by as much as 10–20 °C (Zang et al., 2018; Lembrechts et al., 2020) due to effects such as snow cover (e.g., Evans et al., 2022; von Oppen et al., 2022), vegetation cover (e.g., Lu et al., 2019; Liang et al., 2019; von Oppen et al., 2022), and aridity/relative humidity (e.g., Pérez-Angel et al., 2020; Wang and Liu, 2021). The use of in situ soil temperatures instead of air temperatures has been shown to improve brGDGT calibration performance (Anderson et al., 2014; Wang et al., 2016; Nieto-Moreno et al., 2016; Pérez-Angel et al., 2020; Wang et al., 2020; Wang and Liu, 2021). However, datasets containing both brGDGT distributions and continuous records of corresponding soil temperatures are relatively rare.

The seasonality of the temperature signal recorded by brGDGTs presents another challenge for calibration efforts. Initially, mean annual temperatures were used for global-scale calibrations (e.g., Weijers et al., 2007b). However, it was demonstrated that in regions with substantial seasonality brGDGTs more accurately reflect warm-season rather than annual temperature averages (e.g., Rueda et al., 2009; Peterse et al., 2012; Naafs et al., 2017; Dearing Crampton-Flood et al., 2020). It has been posited that this seasonal bias is due to bacterial growth being slowed at cold or freezing temperatures (e.g., Weijers et al., 2007c). Indeed, the mean temperature of months above freezing (MAF) has recently emerged as the highest performing air temperature index in global brGDGT datasets for both soils (Dearing Crampton-Flood et al., 2020) and lake sediments (Raberg et al., 2021a; Martínez-Sosa et al., 2021).

Additionally, other effects can convolute the link between brGDGTs and temperature. Soil chemistry (De Jonge et al., 2014; Halffman et al., 2022), salinity (Zang et al., 2018), soil water content (SWC; Dang et al., 2016), oxygen availability (Weber et al., 2018), and changes in bacterial community composition (De Jonge et al., 2019) may all influence the relationship between brGDGTs and temperature, though the basic relationship between the two appears to be nearly universal (Raberg et al., 2022b). In lake sediments, the influences of some of these parameters on brGDGT distributions were deconvolved by grouping the lipids into "structural sets" based on their variations in methylation number, methylation position, and cyclopentane ring number (Raberg et al., 2021a). Using these groupings, the temperature influence was shown to be encoded almost entirely by brGDGT methylation number, while pH and conductivity were linked to ring number and methylation position. However, this approach has yet to be applied to soils.

Furthermore, a multitude of brGDGT isomers and related tetraethers exist that have only recently become methodologically resolvable (e.g., Liu et al., 2012; De Jonge et al., 2013; Ding et al., 2016). Our understanding of the role these compounds play in the relationship between brGDGTs and environmental parameters is constantly evolving. For example, the relative abundance of 5- and 6-methyl brGDGT isomers has been linked to aridity and pH (e.g., Xiao et al., 2015; Dang et al., 2016), while the more recently characterized 7-methyl isomers have been shown to relate to salinity in lakes (Wang et al., 2021; Kou et al., 2022). Additionally, a mixed 5-, 6-methyl isomer of brGDGT IIIa, named IIIa'', was found to have methanogenic origins in anoxic lake bottom waters (Weber et al., 2015; Weber et al., 2018). Furthermore, a suite of sparsely and overly branched GDGTs (SB- and OB-GDGTs) have been characterized (Liu et al., 2012), but their environmental and/or phylogenetic controls have been relatively underexplored.

Here, we report brGDGTs distributions from 68 soils from the Eastern Canadian Arctic (ECA) and Iceland. For 51 of these samples, we additionally measured *in situ* soil temperatures for 1–2 years. We compile our results with those of other calibration efforts in China (Wang et al., 2020; Wang and Liu, 2021), Iceland (De Jonge et al., 2019), Scandinavia (Halffman et al., 2022), and Colombia (Pérez-Angel et al., 2020) to generate global, *in situ* soil temperature calibrations for brGDGTs. We further examine the links between brGDGTs and pH, SWC, and electrical conductivity using both the 15 commonly measured brGDGTs and the more recently reported 7-methyl and IIIa'' isomers. We find that the 15 commonly measured brGDGTs most accurately reflect mean summer soil temperature (MSST) and pH, while the 7-methyl and IIIa'' isomers provide insight on seasonal soil microenvironments. We also report the presence or absence of a heptamethyated GDGT with $m/z = 1064$ (OB-GDGT$_{1064}$) and discuss its potential utility in future calibration efforts. Finally, we test our new calibrations on a previously published loess/paleosol sequence (LPS) from the Chinese Loess Plateau (CLP; Lu et al., 2019; Zeng and Yang, 2019) and find that our reconstructions are consistent with the known climate history of the area.

2. Materials and methods

2.1. Study regions and sampling

We collected soil samples at 0–10 cm depth from the Eastern Canadian Arctic (ECA; n = 44) and Iceland (n = 24) in the summers of 2015–2019 (Fig. 1). For 27 soil sites in the ECA and all soil sites in Iceland, we deployed in situ soil temperature loggers (Thermochron DS1925L or DS1922L iButtons, Maxim Integrated Products, accuracy ± 0.5 °C from −40 °C to +85 °C) at 10 cm depth for 1 to 2 years (362 – 727 days). All loggers had a 1- to 3-hourly sampling interval except for four deployed at sites CF3 and CF8 in the ECA, which had a 6-hour sampling interval. Monthly averages for each logger were computed using the full available date ranges. To ensure that the 6-hour sampling interval of some ECA samples was sufficient to reliably calculate monthly temperature averages, we applied the following method. We selected all soils from the ECA with hourly sampling resolution. We then generated 6 subsets of this temperature data at 6-hourly resolution (offset from one another by 1 h) and calculated monthly averages from each of these subsets. Monthly averages calculated from the hourly and 6-hourly datasets had a mean offset of no more than 0.001 ± 0.08 °C, with a maximum offset of 0.13 °C (BIR Soil 9, August 2019). These offsets are well within the accuracy of the temperature loggers (±0.5 °C). A subset of the soil temperature data for 22 soils from the ECA was the subject of a previous study (Evans et al., 2022). Raw soil temperature data has been previously archived (Raberg et al., 2021b; Raberg et al., 2022c).

We measured the pH of all ECA and Iceland soils using an Oaktan pH 150 m with a WD-35614-30 probe. Soil pH was measured using milli-Q water in a 1:2.5 (w:w) soil:water ratio. New containers were used for each soil and the pH meter was calibrated using pH 4.00, 7.00, and 10.00 buffer solutions every 5–10 samples. Electrical conductivity was measured with a SevenEasy conductivity meter (Mettler Toledo) at a 1:5 (w:w) soil:water ratio, with a calibration solution checked every 15–20 samples. SWC, calculated as the percent of the sample mass that was lost

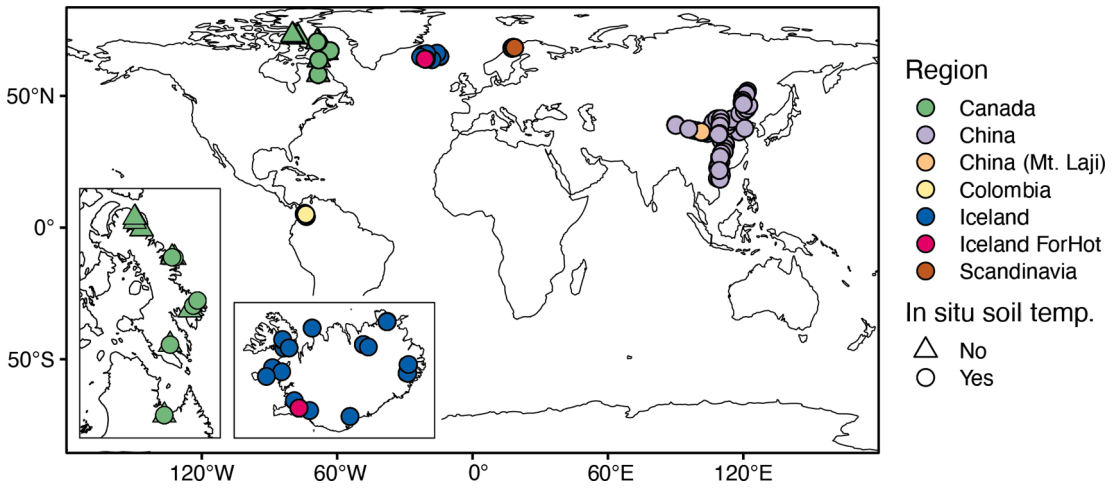

Fig. 1. Map of sites included in this study. Green and blue: Canada and Iceland (this study; see insets); pink, n = 28: de Jonge et al. (2019); yellow, n = 30: Pérez-Angel et al. (2020); brown, n = 37: Halffman et al. (2021); purple, n = 149: Wang et al. (2020); orange, n = 12: Wang and Liu (2021). All sites have associated in situ soil temperature measurements (circles) except for 17 sites in Canada (triangles).

after freeze drying (SWC = (mass wet soil − mass dry soil)/mass dry soil × 100), was measured for all soils from Iceland and 15 soils from the ECA.

To supplement the ECA and Iceland datasets, we also compiled results from published studies containing soil brGDGTs with associated in situ soil temperatures (Fig. 1). These include 37 soils from altitudinal transects in Scandinavia (Halffman et al., 2022), 30 soils from geothermal transects in Iceland (Sigurdsson et al., 2016; De Jonge et al., 2019), 12 soils from an altitudinal transect in China (Mt. Laji; Wang and Liu, 2021), 30 soils from an altitudinal transect in the tropical Andes of Colombia (Pérez-Angel et al., 2020), and 149 soils from a regional study in China (Wang et al., 2020). Where data were available (n = 97), monthly mean soil temperatures were calculated from hourly data that was either previously published (Sigurdsson et al., 2016; Halffman et al., 2022; Halamka et al., 2022) or provided through personal communication with the authors (L. Pérez-Angel; C. de Jonge). Monthly, seasonal, or annual soil temperatures for the remaining samples were compiled as available from published studies and through personal communication with the authors (H. Wang and W. Liu).

Where data were available, we calculated mean annual soil temperature (MAST), the mean soil temperature of all months above freezing (MAFS), mean summer soil temperature (MSST, defined as the mean temperature of the warmest quarter or, due to data availability constraints, the mean of June, July, and August for sites at Mt. Laji, China), mean winter soil temperature (MWST, defined as the mean temperature of the coldest quarter or the mean of December, January, and February for sites at Mt. Laji, China), the warmest month soil temperature (WMST), the coldest month soil temperature (CMST), the soil summer warmth index (SWIS, calculated as the sum of all monthly soil temperature means above freezing), and the soil temperature seasonality (calculated as the difference between the WMST and CMST (Kwiecien et al., 2022)). Where sub-daily soil temperature data were available, we additionally calculated the mean soil temperature of all days above freezing (DAFS) and growing degree days above 0 °C (GDD0S, calculated as the sum of all mean daily soil temperatures above freezing). The resulting dataset consists of 326 samples. Of these, 309 have an associated MAST, 172 have associated seasonal temperatures (e.g., MSST), 160 have associated monthly mean soil temperatures, and 117 have soil temperatures at sub-daily resolution.

Finally, we generated monthly air temperatures for all ECA and Icelandic sites in this study following the methods of Raberg et al. (2021). Briefly, for soils from six lakes in the ECA (BIR, BRO, QPT, CF8, ARQ, and SAL), we used a transfer function to convert 2 m air temperatures recorded by iButton temperature loggers to 30-year climate normals (1971–2000) using data from nearby meteorological stations (Department of Environment, Government of Canada). For all other samples, we used the WorldClim database (Fick and Hijmans, 2017) to generate 30-year (1970–2000) air temperature climate normals. For each soil temperature parameter above, we calculated an analogous air temperature parameter (e.g., mean annual air temperature (MAAT)).

2.2. BrGDGT extraction, characterization, and definitions

Soil samples (1.0–10.0 g) were freeze dried and extracted using a modified Bligh and Dyer method (Bligh and Dyer, 1959; Wörmer et al., 2013; Raberg et al., 2022a). Briefly, soils were first vortexed and sonicated in solvent Mix A (dichloromethane (DCM):methanol (MeOH):50 mM phosphate buffer (aq., pH 7.4) [1:2:0.8, v:v:v]). The mixture was then centrifuged and the supernatant collected. The process was repeated once more with Mix A, followed by two iterations with Mix B (DCM:MeOH:5% trichloroacetic acid buffer (aq., pH 2) [1:2:0.8, v:v:v]) and one with Mix C (DCM:MeOH [1:5, v:v]). The supernatants were combined and separated into organic and aqueous phases using a separatory funnel and equal additions of HPLC-grade water and DCM. The organic fraction was then dried under a gentle stream of N_2 and aliquots were redissolved in 99:1 (v:v) hexane:isopropanol and filtered (0.45 μm, PTFE) before analysis.

To analyze brGDGTs, we used a Thermo Scientific UltiMate 3,000 high-performance liquid chromatography instrument coupled to a Q Exactive Focus Orbitrap-Quadrupole high-resolution mass spectrometer (HPLC-MS) in full scan mode. We used a slightly modified version (Raberg et al., 2021a) of the chromatographic methods established by Hopmans et al. (2016), and identified brGDGTs based on their characteristic masses and elution patterns. We added a known quantity (1 μg) of C46 GDGT internal standard (Huguet et al., 2006) to the extracts quantify brGDGT yields.

In addition to the 15 commonly measured brGDGTs, we integrated peaks corresponding to 7-methyl brGDGTs (Ding et al., 2016) and IIIa'' (Weber et al., 2015). The 7-methyl brGDGTs co-elute with common lower mass brGDGTs. The naturally occurring heavier isotopes of these lower mass compounds can therefore contribute to the 7-methyl isotope peaks, necessitating a correction be applied (Wang et al., 2021). However, the high mass accuracy of the Orbitrap MS used in our study allows us to distinguish the 7-methyl isomers from the naturally occurring heavy isotopes of other brGDGTs. Specifically, IIIa7 and the heavy isotopes of IIIb' overlap chromatographically, but their masses differ by ≥ 9.5 ppm. IIIb7 and the co-eluting heavy isotopes of IIIc' differ by ≥ 5.8 ppm. Finally, IIa7 and the co-eluting heavy isotopes of IIb differ by ≥

5.9 ppm. As we performed peak integrations with a mass tolerance range of ± 5 ppm, the heavy isotopes of IIIb', IIIc', and IIb were already excluded from the integrations and no correction was necessary. We also reported the presence or absence of overly branched GDGT with a mass of 1064 (OB-GDGT$_{1064}$; Liu et al., 2012), but did not quantify this compound due to the complexity of its chromatogram (Fig. S1; Section 3.2).

Fractional abundances (FAs) for each of the structural sets were defined according to Raberg et al. (2021a). Briefly, brGDGTs were grouped according to the three primary observed structural variations: number of methylations, position of methylations, and number of cyclopentane rings. FAs were then calculated within each of these resulting structural sets. For example, grouping brGDGTs by cyclopentane ring number generates the three subgroups containing compounds with zero, one, or two rings, respectively. FAs calculated within these subgroups highlight variations in methylation number and position while holding cyclopentane ring number constant. Taken together, these subgroups thus form the Meth-Isom Set and its FAs (e.g., fIa$_{MI}$). A full guide of the Structural Sets and equations for calculating their FAs has been previously published (Raberg et al., 2021a).

We used the following definitions for the brGDGT-based indices MBT'$_{5Me}$ and CBT' (De Jonge et al., 2014), IR$_{6Me}$ (Dang et al., 2016), and IR$_{7Me}$ (Martin et al., 2019):

$$MBT'_{5Me} = \frac{(Ia + Ib + Ic)}{(Ia + Ib + Ic + IIa + IIb + IIc + IIIa)} \quad (1)$$

$$CBT' = -\log\left(\frac{Ic + IIa' + IIb' + IIc' + IIIa' + IIIb' + IIIc'}{Ia + IIa + IIIa}\right) \quad (2)$$

$$IR_{6Me} = \frac{(IIa' + IIb' + IIc' + IIIa' + IIIb' + IIIc')}{(IIa' + IIb' + IIc' + IIIa' + IIIb' + IIIc' + IIa + IIb + IIc + IIIa + IIIb + IIIc)} \quad (3)$$

$$IR_{7Me} = \frac{(IIa7 + IIIa7 + IIIb7)}{(IIa' + IIb' + IIc' + IIIa' + IIIb' + IIIc' + IIa + IIb + IIc + IIIa + IIIb + IIIc)} \quad (4)$$

2.3. Statistical methods

Calibrations were performed following the methods of Raberg et al. (2021a) and Pérez-Angel et al. (2020). Briefly, FAs were first calculated for each structural set (Raberg et al., 2021a). For each in situ soil temperature variable (and for pH, SWC, and conductivity), two methods were used to construct multiple linear and quadratic regressions: 1) a stepwise forward selection/backwards elimination (SFS/SBE) method using the MASS package (Venables and Ripley, 2002) and 2) a combinatoric approach using the leaps package (Lumley, 2020), both performed in R (Team R Development Core, 2021). We evaluated the fits using the Bayesian information criterion (Schwarz, 1978), adjusted R^2, and the normalized root mean squared error (NRMSE, calculated as the RMSE divided by the range of the fitting parameter). We applied the additional criterion that each fitting variable in the regression must be significant ($p < 0.01$; Pérez-Angel et al., 2020). Finally, we calculated the skewness using the moments package (Komsta and Novomestky, 2022) in R.

Data points with residuals greater in magnitude than 3 times the RMSE were considered outliers. Different temperature parameters (e.g., MAST and MSST) produced different outliers. Rather than exclude all outliers from calibration efforts, we used the following method. First, calibrations were generated using all samples in the compiled dataset (Dataset S1). The top fits for the top 5 temperature variables all identified Iceland ForHot Soil 5F as an outlier, while two additionally identified ForHot Soil 3F as an outlier. We then reran the calibrations excluding Soil 5F and retested for outliers. The top fits for the top 5 temperature variables then all identified Soil 3F as an outlier. When we reran the calibrations again without Soil 3F, some samples were identified as outliers in 3 of the 5 top calibrations, but no sample was identified by more than one calibration. Therefore, we continued with the dataset, excluding only ForHot Soils 3F and 5F.

2.4. Estimating modern values for the Xifeng loess/paleosol sequence

To test the calibrations generated in this study, we used published data from the Xifeng LPS (Lu et al., 2019; Zeng and Yang, 2019). The MAAT at the Xifeng section is 8.5 °C and the July air temperature is 21 °C (Zeng and Yang, 2019). To convert these values to soil temperatures, we generated linear regressions of MAAT versus MAST (adj $R^2 = 0.97$, $p \ll 0.01$) and warmest month air temperature versus MSST (adj. $R^2 = 0.92$, $p \ll 0.01$) using only the Chinese soils in this dataset. We then applied the resulting linear equations to generate a modern MAST of 11.3 °C and MSST of 21.8 °C at Xifeng. To estimate the modern pH, we selected the subset of modern soils from the compiled dataset that fell within the CLP (latitude between 35 and 37 °N; longitude between 105 and 110 °W; coordinates based on map in Zeng et al. (2019); n = 6) and averaged their pH values. The resulting estimated modern pH was 7.84 ± 0.26.

3. Results

3.1. Soil temperatures of the Eastern Canadian Arctic and Iceland

Samples from the ECA formed the cold end members of the compiled dataset, with a minimum and maximum MAST of −8.8 °C and 3.2 °C, respectively. In contrast, MAST in Iceland was warmer and had a smaller range, spanning 1.6 to 5.0 °C. Summer temperatures also ranged widely in the ECA, with MSST going from 2.8 °C to 12.2 °C. In Iceland, MSST values had a smaller range, with a minimum MSST of 6.7 °C and a maximum of 12.2 °C. Icelandic soils generally stayed close to 0 °C during the winter, while soils in the ECA often experienced extreme negative temperatures (e.g., Fig. 2), with CMSTs as low as −27 °C. Soil temperatures also had high spatial variability in the ECA. The soils with both the lowest and highest MSST in the entire 1400 km transect of the ECA dataset, for example, were found at Birch Lake (BIR), just 400 m apart (Fig. 2).

Soil temperatures were closely related to air temperatures in Iceland, but not in the ECA. For example, MSST was well correlated with MAAT

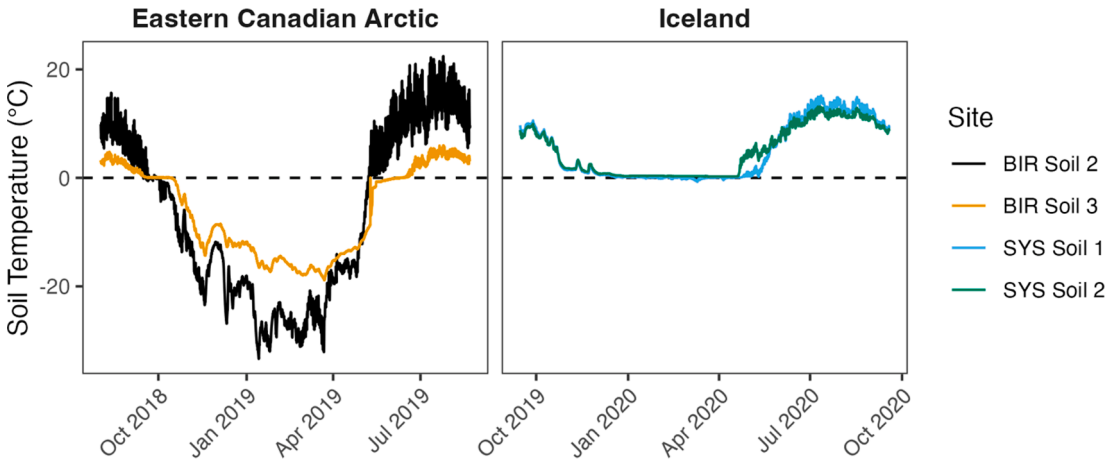

Fig. 2. Representative in situ soil temperature time series from the Eastern Canadian Arctic and Iceland.

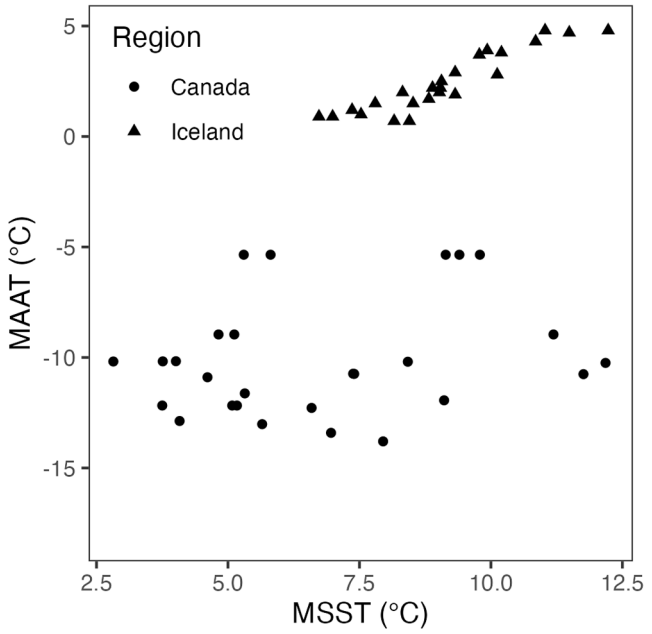

Fig. 3. Mean summer soil temperature (MSST) versus mean annual air temperature (MAAT) for the Eastern Canadian Arctic and Iceland. The two are highly correlated in Iceland (adj. $R^2 = 0.85$, $p \ll 0.01$) but have no significant relationship in the Eastern Canadian Arctic (adj. $R^2 = 0.02$, $p > 0.05$).

in Iceland (adj. $R^2 = 0.85$, p value $<< 0.01$), but the two were uncorrelated in the ECA ($p > 0.05$; Fig. 3). Similarly, winter air temperatures were better predictors of MSST than summer air temperatures in Iceland (adj. $R^2 = 0.87$ and 0.70, respectively, $p << 0.01$ for both). In contrast, neither summer nor winter air temperatures were significantly correlated with MSST in the ECA ($p > 0.05$). Finally, winter soil temperatures were moderately well correlated with winter air temperatures in the ECA (adj. $R^2 = 0.51$, $p \ll 0.01$), but weakly correlated in Iceland (adj. $R^2 = 0.14$, $p < 0.05$).

3.2. BrGDGT distributions

All 15 commonly measured brGDGTs were detected in the Icelandic and ECA datasets (Fig. 4a). IIa and Ia were the most abundant brGDGTs, followed by IIIa and IIa'. In comparison to the other samples in the combined dataset, the Icelandic and ECA soils had a greater proportion of brGDGTs IIIa and IIa and a lower proportion of brGDGT Ia.

BrGDGT IIIa'' was present (Fig. 4b) in 21 of 69 soils, and it exhibited a FA (of all compounds) ≥ 0.01 in 7 of them. The compound was most abundant in soils characterized by high exposure (i.e., little vegetative or topographic shielding from sun or wind), high seasonality, and low vegetation cover; 4 of top 5 FAs were from poorly vegetated ridge tops. The compound was also only present in soils that froze (CMST < 0 °C). For those samples without in situ soil temperatures, it was only detected in 7 of the 8 highest latitude (>72 °N) soils, where the coldest month air temperatures were all < −31 °C. However, not all samples that froze contained IIIa'' and it was not limited to these most extreme settings; it was also present in a forested ECA site (3LN Soil 4) and the warm endmember of the entire ECA-Iceland dataset, a soil site in southern Iceland (VGHV Soil 1). The compound was slightly more common in ECA (16 of 45 soils, 36 %) than Iceland (5 of 24 soils, 21 %).

7-methyl isomers (IIa7, IIIa7, and IIIb7; Ding et al., 2016) were also common in the soils of both Iceland and the ECA. These compounds were similarly associated with barren, high exposure (e.g., ridgetop) settings, but were also present in well-developed organic soils. For soils from the ECA in which 7-methyl compounds were detected, IR_{7Me} values ranged from 0.002 to 0.4, with a mean and standard deviation of 0.05 ± 0.08. In Iceland, these values were lower, ranging from 0.003 to 0.02 with a mean and standard deviation of 0.008 ± 0.002. These are similar to values reported for soils in Mongolia (0.07 ± 0.05; n = 15; Dugerdil et al., 2021) and France (0.02 ± 0.007; n = 10; Martin et al., 2019).

Neither IR_{7Me} nor fIIIa'' were significantly correlated with bulk soil pH, electrical conductivity, or SWC ($p > 0.05$) and were only weakly correlated with temperature parameters (adj. $R^2 \leq 0.37$ and 0.31, respectively). However, the natural log of IR_{7Me} did correlate with soil temperature seasonality (adj $R^2 = 0.65$, $p << 0.01$; Fig. 5a) and cold season soil temperatures (e.g., CMST; adj. $R^2 = 0.58$, $p << 0.01$). Notably, though the natural log of IR_{7Me} was correlated with cold season soil temperatures, it did not correlate with either MSST or WMST ($p > 0.05$). The relationship linking IR_{7Me} and soil temperature seasonality in this study is provided in Eq. (5) (RMSE = 5.80 °C, adj. $R^2 = 0.65$, n = 51):

$$\text{Seasonality } (^{\circ}\text{C}) = 48.7 + 7.24 \times \ln(IR_{7Me}) \quad (5)$$

Additionally, for samples in which IIIa'' was detected, the natural log of fIIIa'' was correlated with IR_{7Me} (adj. $R^2 = 0.84$, $p << 0.01$; Fig. 5b), soil temperature seasonality (adj. $R^2 = 0.76$, $p < 0.01$), MAFS (adj. $R^2 = 0.74$, $p < 0.01$), and SWC (adj. $R^2 = 0.71$, $p < 0.01$), and was more weakly correlated (adj. $R^2 < 0.71$) with other environmental parameters.

Finally, compounds were also detected in the mass range and expected retention time window for OB-$GDGT_{1064}$ (Liu et al., 2012; Fig. S1). This compound and/or its isomers was detected in 20 of 44 samples from the ECA and in all 24 samples from Iceland, often in greater abundance than other commonly measured brGDGTs, such as Ic and IIIb. Due to the complex structure of the peak (presumably due a

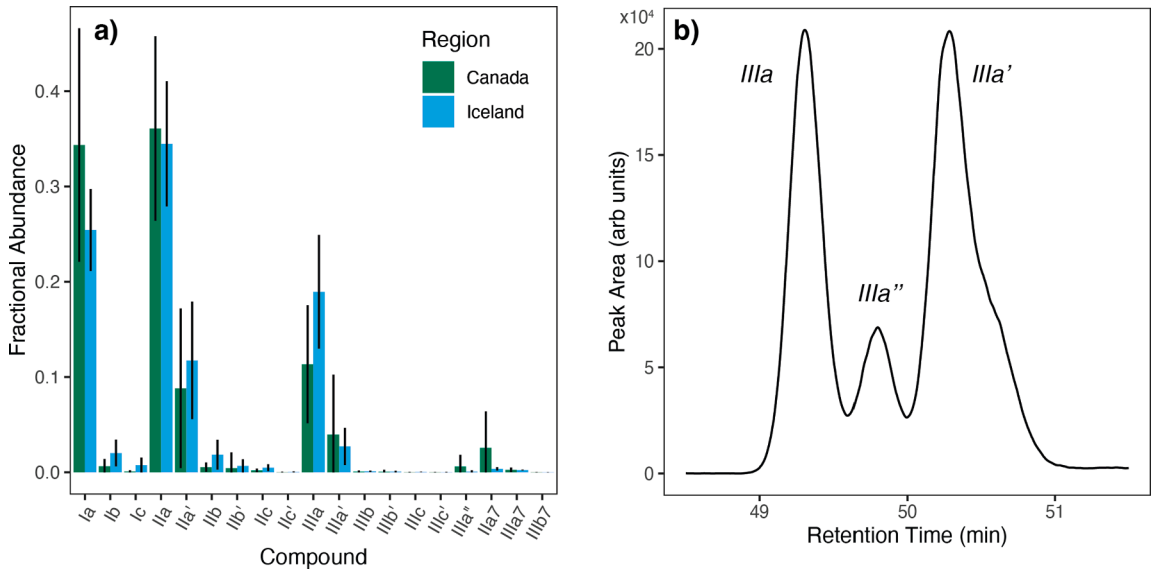

Fig. 4. A) Bar plot of fractional abundances (FAs), including IIIa'' and the 7-methyl isomers identified thus far. Note that FAs in the plot include all measured compounds, while FAs in the calibrations exclude IIIa'' and 7-methyl brGDGTs. B) Extracted ion chromatogram of brGDGTs with a mass-to-charge ratio (*m/z*) of 1050, including the putative lacustrine anoxic biomarker, IIIa'', from a representative soil sample.

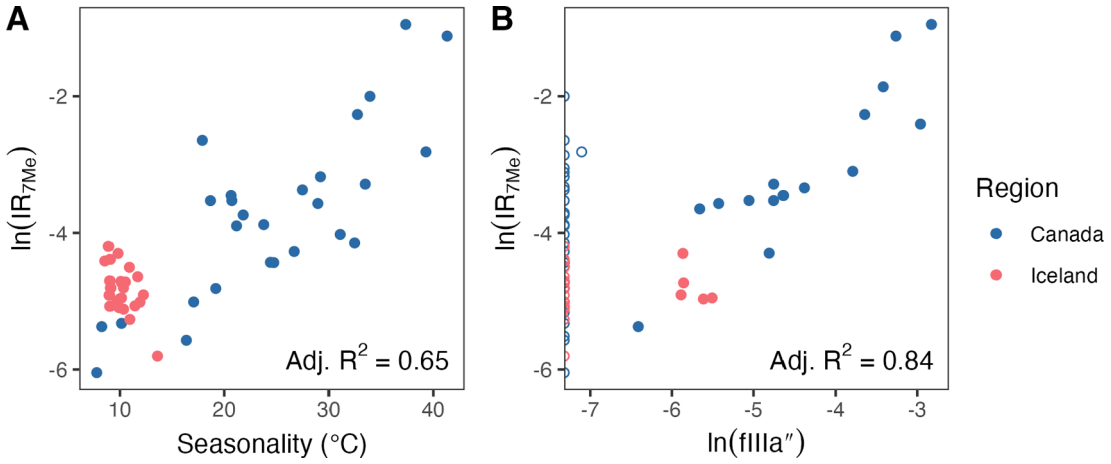

Fig. 5. A) Relationship between seasonality (range of monthly soil temperature averages) and the natural log of IR_{7Me}. B) Relationship between the natural logs of fIIIa'' and IR_{7Me}. Samples with fIIIa'' = 0 are represented with open circles were removed from the correlation in B), along with one outlier. P values were ≪ 0.01 for both plots.

high number of possible isomers; Fig. S1), we did not integrate the compound at this time and report only its presence/absence. Though OB-GDGTs have been associated with anoxia in marine (Xie et al., 2014; Liu et al., 2014) and terrestrial (Lü et al., 2019) environments, its presence here was independent of IIIa''.

3.3. Soil temperature and pH calibrations

We regressed each temperature variable against the structural set FAs (Raberg et al., 2021a) and MBT'_{5Me}. DAFS and GDD0S produced the highest-performing fits in terms of NRMSE, while their monthly counterparts, MAFS and SWIS, produced the highest-performing fits in terms of adjusted R^2. However, examination of these fits showed them to be highly skewed towards the cold end (e.g., Fig. 6a–b), making them sensitive to a limited number of warmer soils and decreasing their ability to distinguish between soils in colder regions. In contrast, temperature variables such as MSST, MAST, and WMST were more evenly distributed, with lower skewness values and greater separation of cold soils (e.g., Fig. 6c). Taking the natural logarithm of GDD0S, DAFS, SWIS, and MAFS decreased their skewness substantially and produced calibrations on par with other top performing fits. However, as an exponentiation of the model output is then required, these calibrations were found to produce highly variable and unrealistic results. We therefore excluded these logarithmic calibrations and focused on temperature variables with a skewness less than 1 for this study.

The highest performing remaining fit, both in terms of NRMSE and adjusted R^2, was for MSST using the Meth-Isom Set FAs (RMSE = 2.07 °C, adj. R^2 = 0.89, n = 164; Fig. 7):

$$MSST(^{\circ}C) = 16.9 - 23.5 \times fIa_{MI}^{2} + 33.7 \times fIa_{MI} - 52.8 \times fIIa_{MI}^{'2} + 31.1 \times fIIa_{MI}^{'} + 86.8 \times fIIa_{MI}^{2} - 69.8 \times fIIa_{MI} - 7.0 \times fIIc_{MI}^{2} + 136.5 \times fIIIa_{MI}^{2} - 42.2 \times fIIIa_{MI} \quad (6)$$

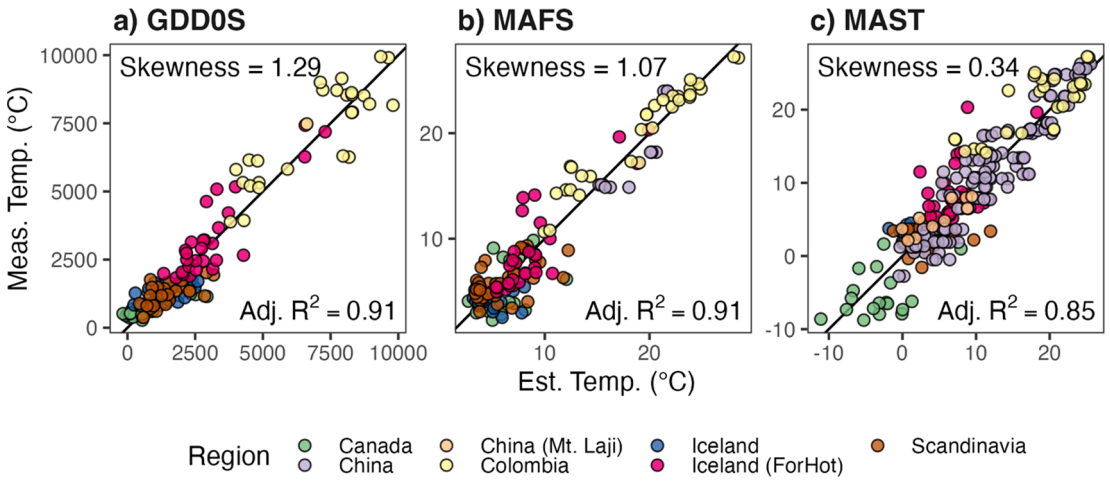

Fig. 6. Estimated versus measured temperatures for three soil temperature variables, showing differing degrees of skewness. A-B) Soil growing degree days above 0 °C (GDD0S) and months above freezing in soils (MAFS) have high adjusted R^2 values, but are highly skewed. C) In contrast, mean annual soil temperature (MAST) has a lower adjusted R^2 value but is more evenly distributed.

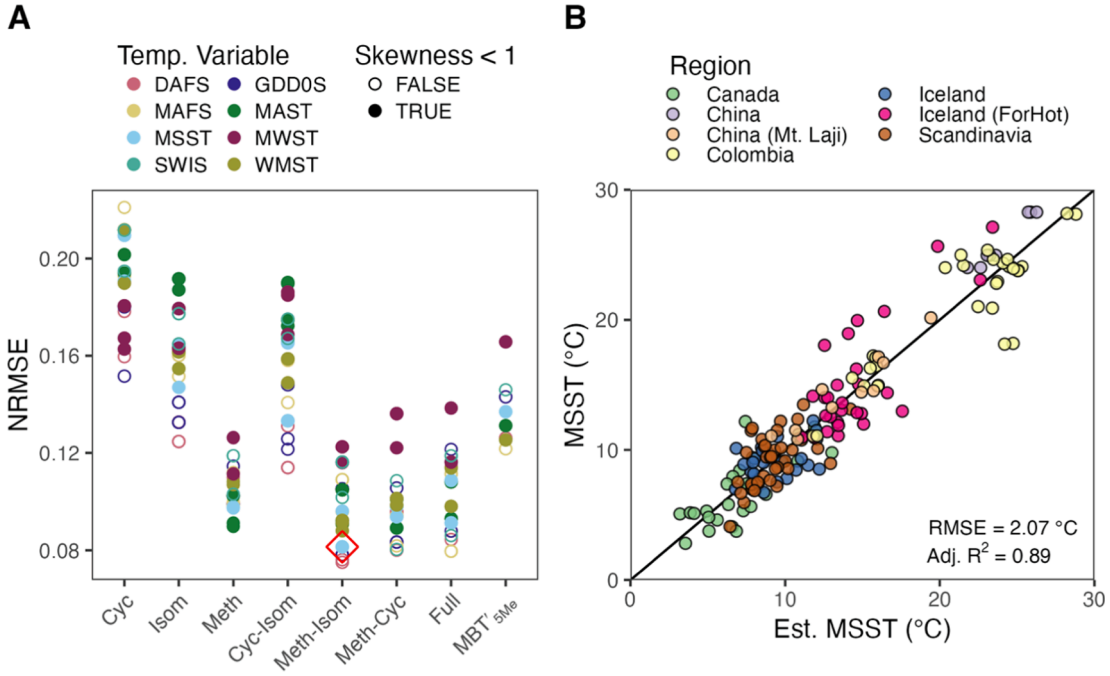

Fig. 7. A) Performance (evaluated using the normalized root mean squared error, NRMSE) of all fits generated using the seven structural sets and MBT'_{5Me} for all tested temperature variables. Fits that were highly skewed (skewness > 1) are shown as unfilled points. The top performing remaining fit (Meth-Isom Set, mean summer soil temperature (MSST); Eq. (6)) is marked with a red diamond in (A) and plotted in (B). "Est. MSST" is the MSST estimated using this fit.

The Meth-Isom Set FAs generated a fit for WMST that performed only marginally worse than that for MSST (RMSE = 2.15 °C, adj. $R^2 = 0.88$, n = 154):

$$WMST(^{\circ}C) = 23.5 + 5.0 \times fIc_{MI} + 45.9 \times fIIa^2_{MI} - 43.8 \times fIIa_{MI} - 7.4 \times fIIb^2_{MI} + 26.5 \times fIIc'_{MI} + 111.0 \times fIIIa^2_{MI} - 47.3 \times fIIIa_{MI}\# \quad (7)$$

Residuals for the MSST and WMST fits showed no significant correlation with pH, conductivity, or SWC ($p > 0.05$).

For MAST, the Meth-Cyc, Meth, and Meth-Isom Sets all produced similarly well-performing calibrations (RMSE = 3.21, 3.24, and 3.28 °C, respectively; adj. $R^2 = 0.85$ for all). However, biases were present in the residuals of the Meth-Cyc Set calibration that could cause it to overestimate temperatures at the cold end of the spectrum and underestimate those at the warm end. We therefore excluded this calibration. The Meth Set calibration (RMSE = 3.24 °C, adj. $R^2 = 0.85$, n = 272) performed slightly better than that of the Meth-Isom Set (RMSE = 3.28 °C, adj. $R^2 = 0.85$, n = 291). However, it was more sensitive to lower abundance compounds such as IIIb' and IIc and may not be appropriate

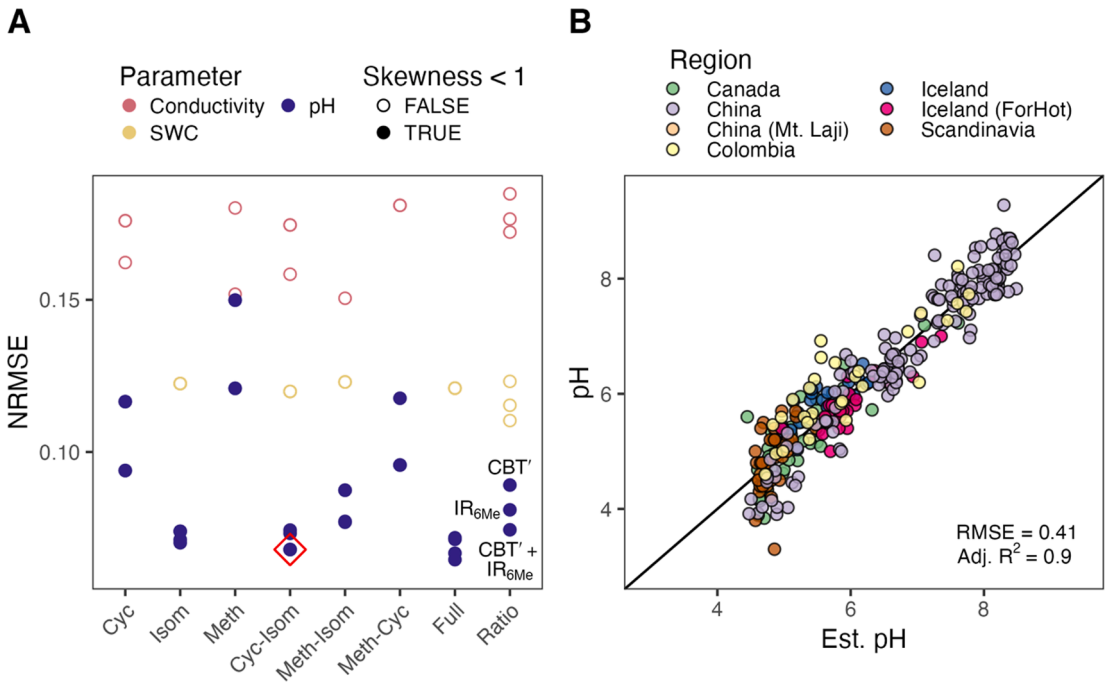

Fig. 8. A) Performance (evaluated using the normalized root mean squared error, NRMSE) of all fits generated using the seven structural sets and defined ratios (CBT', IR_{6Me}, and CBT' + IR_{6Me}; points labeled on plot) for pH, electrical conductivity, and soil water content (SWC). Fits that were highly skewed (skewness > 1) are shown as unfilled points. The Cyc-Isom Set fit for pH (Eq. (11)) is marked with a red diamond in (A) and plotted in (B). "Est. pH" is the pH estimated using this fit.

for applications where these compounds fall below the detection limit. We therefore present both calibrations:

$$\begin{aligned}\mathrm{MAST}_{Meth}(^{\circ}C) = {} & 16.3 + 10.6 \times fIb^{2}_{\mathrm{Meth}} - 15.1 \times fIc^{2}_{\mathrm{Meth}} + 16.3 \times fIc_{\mathrm{Meth}} - 35.1 \times fIIa_{\mathrm{Meth}} - 10.3 \times fIIc_{\mathrm{Meth}} \\ & +23.8 \times fIIIa'^{2}_{\mathrm{Meth}} - 28.3 \times fIIIa'_{\mathrm{Meth}} - 14.4 \times fIIIb'^{2}_{\mathrm{Meth}} + 12.7 \times fIIIb'_{\mathrm{Meth}} + 12.7 \times fIIb^{2}_{\mathrm{Meth}}\end{aligned} \quad (8)$$

$$\begin{aligned}\mathrm{MAST}_{MI}(^{\circ}C) = {} & 5.5 - 39.9 \times fIa^{2}_{\mathrm{MI}} + 60.6 \times fIa_{\mathrm{MI}} - 12.8 \times fIc^{2}_{\mathrm{MI}} + 12.9 \times fIc_{\mathrm{MI}} + 98.4 \times fIIa^{2}_{\mathrm{MI}} - 88.1 \times \\ & fIIa_{\mathrm{MI}} - 12.3 \times fIIc_{\mathrm{MI}} + 100.9 \times fIIIa^{2}_{\mathrm{MI}}\end{aligned} \quad (9)$$

BrGDGTs were not as good of a predictor of winter soil temperatures (CMST, adj. $R^2 = 0.75$; MWST, adj. $R^2 = 0.74$) or any air temperature parameter (highest performing fit: MAF, adj. $R^2 = 0.85$).

Calibrations for SWC and conductivity were weak (adj. $R^2 = 0.28$ and 0.36, respectively; Fig. 8). However, strong fits were produced for soil pH using the Full, Cyc-Isom, and Isom Sets (adj. $R^2 = 0.91$, 0.90, and 0.89, respectively; Fig. 8). The Isom Set calibration relied on low abundance compounds such as IIIb' and IIIc' though, limiting its utility. Thus, we report the calibrations for Full (RMSE = 0.39, adj. $R^2 = 0.91$, n = 312) and Cyc-Isom (RMSE = 0.41, adj. $R^2 = 0.90$, n = 312) Sets:

$$\begin{aligned}\mathrm{pH}_{Full} = {} & 18.8 - 13.9 \times fIa_{\mathrm{Full}} - 29.8 \times fIb^{2}_{\mathrm{Full}} - 9.2 \times fIIa'_{\mathrm{Full}} + 7.4 \times fIIa^{2}_{\mathrm{Full}} - 18.6 \times fIIa_{\mathrm{Full}} - 13.7 \times \\ & fIIb'_{\mathrm{Full}} - 18.8 \times fIIb_{\mathrm{Full}} - 10.7 \times fIIIa'_{\mathrm{Full}} - 11.2 \times fIIIa_{\mathrm{Full}} + 3012.8 \times fIIIb'^{2}_{\mathrm{Full}} - 68.3 \times fIIIb'_{\mathrm{Full}}\end{aligned} \quad (10)$$

$$\begin{aligned}\mathrm{pH}_{CI} = {} & 10.1 + 2.1 \times fIIa'^{2}_{\mathrm{CI}} - 1.9 \times fIIa^{2}_{\mathrm{CI}} - 11.6 \times fIIc_{\mathrm{CI}} + 2.2 \times fIIIa'^{2}_{\mathrm{CI}} - 4.5 \times fIIIa'_{\mathrm{CI}} \\ & -2.2 \times fIIIa_{\mathrm{CI}} - 1.4 \times fIa^{2}_{\mathrm{CI}}\end{aligned} \quad (11)$$

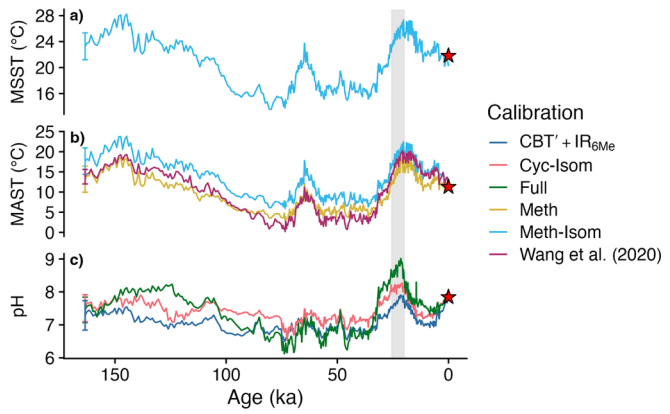

Fig. 9. Application of new calibrations to the Xifeng loess/paleosol sequence (Zeng et al., 2019; Lu et al., 2019). Corresponding equations are as follows: a) Eq. (6) (light blue); b) Eq. (8) (yellow), Eq. (9) (light blue), and Wang et al. (2020) Eq. (8) (maroon); c) Eqs. (10)–(12) (green, pink, and dark blue, respectively). Red stars denote modern values. Error bars (±RMSE) are shown for the oldest points. Gray bar marks a peak in pH that slightly leads a peak in temperature.

We also found that both CBT' and IR_{6Me} were good predictors of soil pH, particularly when the two are used in a linear combination (RMSE = 0.44, adj. $R^2 = 0.88$, n = 312):

$$pH_{CBT',IR6Me} = 5.51 + 0.55 \times CBT' + 2.41 \times IR_{6Me} \quad (12)$$

However, we note that biases in the residuals for the pH fits appear below pH ~ 4.6 that would cause the calibration to overestimate pH (e.g., Cyc-Isom Set; Fig. 8b). Therefore, caution should be taken in applying these calibrations at low pH (< ~ 4.6).

As reported for lake sediments (Raberg et al., 2021a), methylation number was identified as the key structural variable responsible for the temperature dependence of brGDGTs in soils; holding methylation number constant, as in the Cyc, Isom, and Cyc-Isom Sets, greatly reduced calibration performance (Fig. 7a). Similarly, methylation position, captured either by the Isom Set or IR_{6Me}, was the most important structural variable in pH calibrations, followed by ring number, as captured by the Cyc Set and CBT' (Fig. 8a). Combining the two via the Cyc-Isom Set or a linear combination of CBT' and IR_{6Me} provided the strongest pH fits. Methylation number, in contrast, was a poor predictor of pH (Meth Set in Fig. 8a). These results were in agreement with lake sediment calibrations (Raberg et al., 2021a) and broader trends across global sample types (Raberg et al., 2022b).

3.4. Application to the Xifeng loess/paleosol sequence

To test their performance, we applied our calibrations for MSST (Eqn. (6), MAST (Eqs. (8) and (9)), and pH (Eqs. (10)–(12)) to the Xifeng LPS from the CLP (Lu et al., 2019; Zeng and Yang, 2019; Fig. 9). Furthermore, for comparison, we applied a previously published regional Chinese MAST calibration (Wang et al., 2020; Fig. 9b). All calibrations reproduced inferred modern temperature and pH values from modern surface samples (red stars in Fig. 9). Additionally, MSST and MAST reconstructions were in good qualitative agreement with one another and broadly aligned with key trends observed in previous work (Lu et al., 2019), with peak temperatures occurring during the Last Glacial Maximum (LGM ~21–17 ka; Fig. 9a–b). Where multiple calibrations were applied, differences of as much as ~5 °C (MAST) and ~1 unit (pH) were present in the downcore record. A prominent peak in pH values (~20–26 ka; gray bar in Fig. 9) was present that slightly led the peak temperatures reconstructed during the LGM.

4. Discussion

4.1. In situ soil temperatures versus air temperatures

The soils of the ECA (the coldest end-members) highlighted the importance of using in situ soil temperatures instead of air temperatures in brGDGT calibrations. Variations in snowpack, microtopography, and vegetation cover were likely drivers of the high spatial variability in observed soil temperatures (Loranty et al., 2018; Evans et al., 2022; Heijmans et al., 2022). Despite having the same air temperature, for example, a pair of soils just 400 m apart at Birch Lake had the warmest and coldest MSST values in the entire ECA dataset, differing by more than 9 °C. The offset between these soils was even larger in winter, with an MWST difference of 10 °C. Such soil-air temperature offsets and spatial variability were common in our dataset and highlight the limitations of using air temperatures for generating brGDGT soil calibrations and in lipid biomarker studies in soils more broadly.

These soil-air offsets must be taken into consideration not only when generating calibrations, but also when applying them in paleoclimate reconstructions. For example, MSST was strongly correlated with MAAT in Iceland (Fig. 3). Paleotemperatures reconstructed from soil brGDGTs in that region could therefore be converted with some confidence to MAAT values for comparison with other proxies and/or model outputs. However, the same approach could not be taken in the ECA, where MSST and MAAT showed no significant relationship (Fig. 3). In mountainous regions, such as the Eastern Cordillera of Colombia and Mt. Laji in China, soil temperatures were closely linked to air temperatures, but with an offset that grew with elevation (Pérez-Angel et al., 2020; Wang and Liu, 2021). Finally, in the Xifeng LPS, the warmest soil temperatures were counterintuitively produced during the Last Glacial Maximum (Fig. 9; see Section 4.4 for discussion). A regional (and temporal) understanding of the connection between soil and air temperatures is thus paramount for interpreting paleotemperature records generated from in situ soil temperature calibrations.

Finally, we note that while the soil temperatures used in this and other studies are likely to be more representative of the temperature regimes experienced by brGDGT-producing bacteria than air temperatures, they carry their own sources of uncertainty. Limited (1- to 2-year) and often non-overlapping (e.g., 2017–2018 versus 2018–2019) temporal ranges make the soil temperature data vulnerable to uncertainties associated with interannual variability. Given the roughly decadal turnover rates of brGDGTs in soils and peats (Weijers et al., 2010; Peterse et al., 2010; Weijers et al., 2011; Huguet et al., 2017), longer-term averages of soil temperatures (e.g., 30-year climate normals) would be ideal for calibration efforts. However, such records are rare. Furthermore, published data currently consist of soil temperatures measured at 2, 5, 10, and 50 cm depths. While soil samples taken for brGDGT analyses reflect those depths (e.g., Halffman et al. (2022) paired 2 cm temperatures with soils sampled from 0 to 5 cm), these slight methodological differences may contribute to calibration uncertainty. Such considerations may help to guide further geochemical studies relying on in situ soil temperature measurements.

4.2. Temperature dependence of brGDGT distributions

BrGDGT distributions in soils from the ECA and Iceland broadly align with global trends, with more highly methylated compounds (hexa- and penta-methylated brGDGTs) appearing in greater relative abundance than is typically observed in warmer climates. Furthermore, we detected an even more highly methylated tetraether in our sample set, OB-$GDGT_{1064}$. As the logical next compound in the Ia-IIa-IIIa series, this heptamethylated tetraether could also be renamed "brGDGT-IVa" and tested in temperature calibration efforts, especially in cold regions. However, the complexity of the detected peak (Fig. S1) calls for careful structural and chromatographic characterization before such efforts can be undertaken. Additionally, while its structural similarities and

association with brGDGTs suggest a similar biological origin (Liu et al., 2012; Lü et al., 2019), the producers of OB-GDGTs remain unknown. Regardless, its presence in the soils of the ECA and Iceland extends the known range of this compound beyond the anoxic marine (Xie et al., 2014; Liu et al., 2014) and wetland (Lü et al., 2019) environments in which it has previously been discovered and encourages broader surveys of tetraether lipids in soils.

BrGDGTs recorded warm season soil temperatures in the compiled dataset. The Meth-Isom Set FAs produced the highest-performing fits, with MSST emerging as the most accurately reproduced temperature variable (Fig. 7b). This calibration performed well for the combined dataset and was significant when applied to each region independently ($p < 0.05$ for Iceland; $p < 0.01$ for all other regions). In particular, the calibration appears likely to perform well on the cold end of the temperature spectrum, with samples from all regions in good agreement and well distributed along the calibration one-to-one line (Fig. 7b). The warm end of the calibration consisted of fewer samples and had more scatter. This may imply that the in situ soil calibration presented here could be improved by the addition of samples on the warm end of the temperature spectrum or that brGDGTs may more accurately record a temperature parameter other than MSST in warm climates. We note that tropics-specific soil calibrations have previously been developed for such climates (Pérez-Angel et al., 2020).

The fact that MSST was the highest-performing temperature parameter in our study may suggest that soil brGDGT production is biased towards the summer. However, it is unlikely that such production is limited to these three warmest months of the year. Indeed, previous studies relating soil brGDGTs to air temperatures have found the temperatures of the months above freezing (i.e., GDD0 and MAF) to provide high performing calibrations (Naafs et al., 2017; Dearing Crampton-Flood et al., 2020; Véquaud et al., 2022). The analogous soil temperature parameters (GDD0S, SWIS, MAFS, and DAFS) provided some of the highest performing fits in this study as well (Fig. 7a), but all had a high skewness due to limited data availability and were therefore excluded. This gap in the available data highlights the need for more paired measurements of brGDGTs and in situ soil temperatures, especially from mid-to-low latitudes, and necessitates caution when applying our calibrations in these regions.

Apart from MSST, we also presented high performing fits for WMST and MAST, which both had skewness < 1. While these calibrations performed slightly worse than that generated for MSST, they may prove useful for comparison with other proxies or for converting between reconstructed soil and air temperatures (Section 4.1).

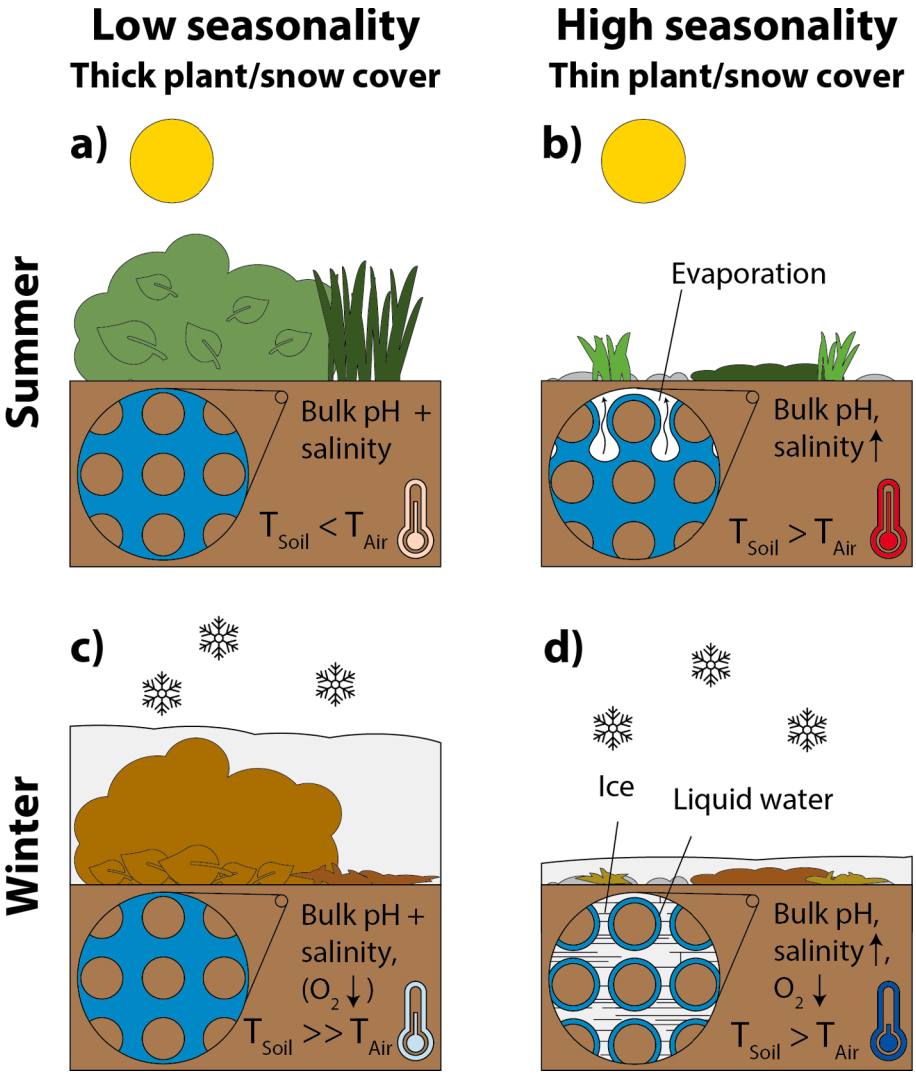

Fig. 10. Schematic of soil conditions experienced by brGDGT-producing bacteria for a), c) low seasonality and b), d) high seasonality soils in a-b) summer and c-d) winter conditions. Salinity is increased in high seasonality soils in both summer (b) and winter (d) by evaporation and freezing, respectively, while pH is likely to be unchanged due to buffering. Soil temperatures can be less than air temperatures due to shading (a) or greater than air temperatures due to direct absorption of solar radiation (b) or insulation from thick and porous (c) or thin and dense (d) snow cover. Decreased connectivity between the soil and atmosphere in winter can lead to oxygen depletion in c) and d).

In a previous calibration of brGDGTs in lake surface sediments, it was found that the Structural Set approach highlighted the importance of brGDGT methylation number in temperature calibrations (Raberg et al., 2021a). In that study, calibrations constructed from Structural Sets in which methylation number was held constant (Cyc, Isom, and Cyc-Isom) had lower adjusted R^2 values than those generated from sets that allowed methylation number to vary (Meth, Meth-Isom, Meth-Cyc, and Full). This finding in lake sediments was mirrored in the soils of this study; calibrations from the Meth, Meth-Isom, Meth-Cyc, and Full Sets outperformed those generated using the Cyc, Isom, and Cyc-Isom Sets (Fig. 7a). Though the MBT'_{5Me} index also captures variations in methylation number, linear calibrations generated using this index did not perform as well as those generating using brGDGT FAs (Fig. 7a). Overall, these results support previous work suggesting a physiological underpinning to the brGDGT temperature proxy (Raberg et al., 2022b), encouraging its application in paleoclimatological studies.

4.3. Relationships between brGDGTs and soil chemistry

BrGDGTs showed a strong relationship with soil pH (Fig. 8). This relationship was primarily driven by changes in cyclopentane ring number and methylation position, as has been observed in previous studies for soils and lakes (e.g., Weijers et al., 2007b; Xiao et al., 2015; Raberg et al., 2021a; Fig. 8a). While ring number was a stronger predictor of pH in lake sediments, methylation position appeared to be more important in soils (Fig. 8a). A combination of the two structural variables via the Cyc-Isom Set FAs or a linear combination of the IR_{6Me} and CBT' indices produced the highest performing calibrations in our dataset (Eqs. (11) and (12)).

In addition to bulk soil pH, the properties of seasonal soil microenvironments may have been recorded in the ECA and Icelandic soils via the abundances of 7-methyl brGDGT isomers and IIIa''. 7-methyl brGDGTs in lake sediments have been shown to correlate with lake water salinity (Wang et al., 2021; Kou et al., 2022) and sediment pH (Ding et al., 2016). In our dataset, however, no significant correlations were present for either IR_{7Me} or its natural log with electrical conductivity, pH, or SWC ($p > 0.05$). This lack of correlation could indicate that 7-methyl isomers are sensitive to different environmental controls in soils and lakes. However, it could also arise due to a mismatch between bulk measurements and the actual soil microenvironments inhabited by brGDGT-producing bacteria.

With monthly soil temperature averages as low as −27 °C and seasonality values as high as 41 °C, soils from the ECA were the extreme end members of this dataset. Such conditions generally developed in conjunction with a lack of vegetation cover; without taller plants like shrubs to shield incoming solar radiation in the summer and to hold an insulating blanket of snow in the winter, these soils experienced both hot and cold temperature extremes (e.g., Zhang, 2005; Kropp et al., 2021; Evans et al., 2022; Heijmans et al., 2022; Fig. 10). Under such conditions, soil water salinity can fluctuate seasonally. In the summer, the loss of water through evaporation can cause an increase in ion concentrations (Fig. 10b). In the winter, a similar concentration of ions can occur as interstitial soil water freezes, leaving behind thin layers of more saline liquid water adsorbed to soil particles (Torrance and Schellekens, 2006; Fig. 10d). Even at temperatures well below 0 °C, the ratio of unfrozen water to dry soil remains between ~0.1 and ~15 % (Romanovsky and Osterkamp, 2000; Sparrman et al., 2004; Öquist et al., 2009). Bacteria, including acidobacteria and other brGDGT candidate producers (Steven et al., 2008; Tuorto et al., 2014), metabolize (Panikov, 2005; McMahon et al., 2009; Segura et al., 2019), reproduce (McMahon et al., 2009; Tuorto et al., 2014), and construct new lipids (Drotz et al., 2010) in the winter by surviving in these unfrozen waters (Panikov et al., 2006; Öquist et al., 2009). Thus, high seasonality drives the development of more saline microenvironments inhabited by active microbial life in both the summer and winter. As the abundance of 7-methyl brGDGTs has been previously shown to correlate with salinity in lakes, the observed correlation between IR_{7Me} and seasonality in this study may in fact reflect the heightened soil water salinity of these seasonal microbial niches. This hypothesis is consistent with the results of Dugerdil et al. (2021), who observed 7-methyl isomers to be primarily associated with steppe or desert landscapes in Mongolia. Finally, in our study, IR_{7Me} was correlated with cold season temperatures but not with summer temperatures. This may suggest that the concentration of ions during winter plays a stronger role in raising soil water salinity than summertime evaporation in these high latitude soils.

The development of seasonal microbial niches may also explain the anomalous presence of IIIa'' in the soils of the ECA and Iceland. IIIa'' has been identified in the sediments of anoxic lakes in Switzerland (Weber et al., 2015; Weber et al., 2018) and France (Martin et al., 2019), but was notably absent in their surrounding soils. It was further shown to be uniquely associated with methanotrophy in anoxic lake bottom waters (Weber et al., 2018) and has been used as a proxy for the development of anoxia in paleoclimate reconstructions (Martin et al., 2019; Rodrigo-Gámiz et al., 2022). Its presence in the soils of the ECA and Iceland was therefore unexpected. It is possible that the environmental conditions driving its production in soils differ from those in lakes. However, it is also possible that the compound is indicative of low oxygen conditions via the seasonal development of anoxic microenvironments in otherwise well-aerated soils.

Freezing both hinders the transport of oxygen from the atmosphere and concentrates nutrient supplies in surviving pore waters, driving the development of anoxic conditions and heightening anaerobic microbial activity in soils (Yu et al., 2007). In our dataset, IIIa'' was only present in soils that froze. Furthermore, where IIIa'' was present, it was highly correlated with the log of IR_{7Me} (Fig. 5b). These results are consistent with the development of anoxia in isolated niches of habitable water within the frozen soil matrix. We also note, however, that not all soils that froze and/or had high IR_{7Me} values contained IIIa'', indicating that other environmental factors, such as organic matter availability or microbial community composition, may be pertinent. Finally, given that we lack direct measurements of soil oxygen levels in this study, it is also possible that IIIa'' is not in fact linked to anoxia in soils and is produced in response to other (unmeasured) environmental conditions entirely, motivating further research into the presence of this compound in soils.

Finally, we note that our hypothesis implies the wintertime production of soil brGDGTs, in apparent conflict with well-documented warm-season biases. The production of brGDGTs in winter would imply that some quantity of cold-biased brGDGTs contributes to the overall lipid pool, potentially skewing brGDGT-inferred temperatures towards the cold end. While it is not possible to quantify this effect in this study, the low relative abundance of 7-methyl and IIIa'' isomers (Fig. 4) along with the robust summer temperature calibrations (Fig. 7) suggest that this winter contribution is small.

If our hypothesis is correct, lipids such as these 7-methyl and IIIa'' isomers may also find broader utility in more detailed studies of soil microenvironments. Due to their relationships with soil conditions at the micro rather than macro scale, these or other recalcitrant lipids could potentially be used as biomarkers for probing the (transient) conditions experienced by microbes inhabiting small-scale niches in a heterogenous soil matrix.

4.4. Application

BrGDGTs in the Xifeng loess/paleosol sequence of the CLP have been used to reconstruct temperature changes at high resolution over the last >160 ka (Lu et al., 2019; Zeng and Yang, 2019). Peak temperatures at Xifeng appeared during the Last Glacial Maximum (LGM ~21–17 ka; Lu et al., 2019), a seemingly paradoxical result that was explained by the development of relatively arid (Youfeng et al., 2008) and sparsely vegetated conditions on the CLP during the LGM (Lu et al., 2019). Under such conditions, soils on the CLP can be ~10 °C warmer than the air in July, whereas the offset is close to zero for vegetated areas nearby (Lu

et al., 2019). Thus, despite colder conditions globally, land surface temperatures, modulated by aridity and vegetation, became warmer on the CLP. This land–ocean temperature offset was observed on ~3 Ma timescales as well and was linked to the strengthening of the East Asian Monsoon (Lu et al., 2022).

While Lu et al. (2019) recognized that brGDGTs in the Xifeng section were likely to be recording warm-season soil temperatures, only air temperature calibrations were available at that time. Here, we applied our calibrations to directly reconstruct soil temperature at Xifeng. Our MSST reconstruction (Fig. 9a) generated an LGM temperature change that was similar in timing, structure, and magnitude to that reported by Lu et al. (2019), with the onset of warming at ~36 ka, peak temperatures ~ 18 ka, and a ~10 °C temperature change overall, from ~16 to 26 °C. The modern surface sample matched our inferred modern summer soil temperature at Xifeng, highlighting the relative accuracy of our new soil temperature calibrations (red star in Fig. 9a).

We also applied both the Meth and Meth-Isom MAST calibrations to the Xifeng sequence and compared the resulting temperatures to those reconstructed using a regional Chinese in situ soil temperature calibration that is well tailored for use on the CLP (Wang et al., 2020; Fig. 9b). The three calibrations produced similar temperature trends and all reproduced the inferred modern MAST. The fact that the Meth and Meth-Isom Set calibrations, which were generated from globally distributed samples with a wider temperature range (an extra 6 °C on the cold end and 1 °C on the warm end), produced trends that are consistent with the regionally tailored calibration lends confidence to their widespread applicability. However, the magnitudes of reconstructed temperatures differed to varying degrees throughout the record, with values sometimes in agreement and sometimes offset by as much as ~5 °C. These offsets are generally less than the cumulative RMSEs of the calibrations (RMSE = 1.8, 3.24, and 3.28 °C for the Wang et al. (2020), Meth, and Meth-Isom Set calibrations, respectively), but highlight the difficulty in determining the most accurate paleoclimate reconstruction from statistically similar calibrations.

BrGDGTs have also been proposed to reflect precipitation/evaporation balance on the CLP through their connections with pH or SWC (Peterse et al., 2014; Sun et al., 2019; Zheng et al., 2022). We therefore applied our three reported pH calibrations (Eqs. (10)–(12)) to the Xifeng LPS (Fig. 9c). As in the case of MAST, all three calibrations reproduced our inferred modern pH value and showed similar qualitative trends, but often differed in magnitude. Despite their differences, all three calibrations produce a peak in pH from ~20–26 ka that leads the main peak in temperature. Such a decoupling of pH and temperature trends has been previously observed from LPSs on the CLP (Peterse et al., 2014; Lu et al., 2016). As more alkaline soils tend to be associated with more arid conditions (e.g., Slessarev et al., 2016), this increase in pH may be driven by aridification (Sun et al., 2019). Thus, the high soil temperatures and alkaline conditions reconstructed by all calibrations presented here are consistent with previous work proposing that more arid and sparsely vegetated conditions prevailed on the CLP around the LGM.

Finally, while 7-methyl brGDGTs were not reported for the Xifeng LPS, their connection with seasonality could theoretically provide additional insight into the LGM aridification of the CLP. As the landscape transitioned from being well-vegetated to more barren, the accompanying increase in soil temperature seasonality could have driven the development of seasonal niches of higher salinity in soil microenvironments (Fig. 10b). Additionally, a shift in the precipitation-evaporation balance towards more arid conditions would have been likely to increase salinity in the soils beyond seasonal effects alone. These salinity increases could have led to the heightened production of 7-methyl isomers, as recorded by the IR_{7Me} index, and will be valuable to quantify in future studies. Such potential applications highlight the importance of further research into less commonly measured brGDGT isomers and their relationships with the environment.

5. Conclusions

We measured brGDGT distributions, in situ soil temperatures, pH, SWC, and electrical conductivity in soils from the Eastern Canadian Arctic and Iceland. We compiled our results with those from other studies containing in situ soil temperature measurements and used the combined dataset to generate global modern calibrations for brGDGT temperature and pH proxies. The highest-performing temperature calibrations were for warm season soil temperatures, especially Mean Summer Soil Temperature (Eqn. (6)), and for pH (Eqs. (10) and (11)). Soil temperatures outperformed air temperatures in our calibrations, likely due to the large (~10 °C) offsets that can arise between the two in both summer and winter (Section 4.3, Fig. 10). As has been shown in previous studies, methylation number was confirmed to be the most important structural variable in these temperature calibrations, while pH was most strongly related to cyclization number and methylation position. We reported the presence of a heptamethylated tetraether (and its isomers), OB-$GDGT_{1064}$, and suggested that it should be studied for its potential to improve brGDGT calibrations, especially in cold regions.

We additionally applied our new temperature and pH calibrations to the Xifeng Loess-Paleosol Sequence on the Chinese Loess Plateau. All calibrations reproduced inferred modern soil temperature and pH values. Furthermore, they produced qualitatively similar trends across the ~160 ka record, which agreed with previously published analyses. The agreement of our new global calibrations with the ones tailored for the Chinese Loess Plateau encourages their use more broadly. However, despite the qualitative agreement, the magnitudes of reconstructed values often diverged in the record, highlighting the challenges in interpreting paleoclimate records generated from statistically similar calibrations.

Finally, we measured the abundances of the 7-methyl and IIIa'' brGDGT isomers in the ECA and Icelandic soils and hypothesized that they are formed in habitable liquid microenvironments in otherwise frozen soils. 7-methyl isomers have been shown to relate to salinity in lakes (Wang et al., 2021). Though the compounds did not correlate to bulk soil properties such as pH, SWC, or conductivity in our study, they did show a correlation with seasonality and winter soil temperatures. Furthermore, IIIa'', a putative marker of anoxic lake waters, was present in the soils of the ECA and Iceland and was found to correlate strongly with IR_{7Me} where it was present. These results may suggest that brGDGTs are produced in the wintertime in small, habitable niches of more saline, sometimes anoxic, liquid water in an otherwise frozen soil matrix (Fig. 10, Section 4.3).

In conclusion, brGDGT lipids in cold regions record summer soil temperatures and bulk soil pH. They may further record the chemistry of seasonal soil microenvironments through less commonly measured brGDGT isomers. Our findings advance our understanding of the seasonality of brGDGT production and provide new in situ soil temperature and pH calibrations for global use. These advances encourage the continued application and further refinement of paleoenvironmental proxies based on soil brGDGT lipids.

Data availability

Data are available through the Arctic Data Center data repository at https://doi.org/10.18739/A27P8TF8W.

CRediT authorship contribution statement

Jonathan H. Raberg: Writing – review & editing, Writing – original draft, Visualization, Validation, Methodology, Investigation, Formal analysis, Data curation, Conceptualization. **Sarah E. Crump:** Methodology, Funding acquisition, Conceptualization. **Greg de Wet:** Methodology, Conceptualization. **David J. Harning:** Writing – review & editing, Conceptualization. **Gifford H. Miller:** Supervision, Funding acquisition, Conceptualization. **Áslaug Geirsdóttir:** Writing – review &

editing, Supervision, Funding acquisition, Conceptualization. **Julio Sepúlveda:** Writing – review & editing, Supervision, Funding acquisition, Conceptualization.

Declaration of competing interest

The authors declare that they have no known competing financial interests or personal relationships that could have appeared to influence the work reported in this paper.

Acknowledgements

This research has been supported by the National Science Foundation (grant nos. OPP-1737712, OPP-1836981, and DDRI-1657743), the National Geographic Society (grant no. CP-019ER-17), a doctoral grant from the University of Iceland, a project grant from the University of Iceland Research Fund (grant no. 15642), and the University of Colorado Boulder. We thank the Inuit of Nunavut for permitting access to their land and to sample soils and lake sediment (Scientific Research Licenses 01022 17R-M, 02034 18R-M, 02038 19R-M) and the Qikiqtani Inuit of Qikiqtarjuaq and Clyde River for assistance in the field. We thank the Nunavut Research Institute for logistical assistance and the Polar Continental Shelf Project for air support. Field research further benefited from the assistance of Ian Holmen, Sveinbjörn Steinthorsson, Martha Raynolds, Shawnee Kasanke, and Helga Bueltmann. We thank Rebecca McCabe for collecting Bylot Island soils and Nodin de Saillan for collecting many temperature loggers on Baffin Island. We thank Cindy de Jonge, Bjarni Sigurdsson, Huanye Wang, Weiguo Liu, and Lina Pérez-Angel for helpfully providing in situ soil temperature data. We thank Noah Fierer and Sebastian Kopf for helpful discussions about microbial life in frozen soils. Finally, we thank two anonymous reviewers, Associate Editor Xiaojuan Feng, and Executive Editor Jeffrey Catalano for helpful comments that greatly improved the quality of this manuscript. We dedicate this article to the life of Sarah E. Crump, who elevated the personal and scientific lives of all around her and without whom this work would not have been possible.

Appendix A. Supplementary material

Supplementary Figure S1 is provided in the supplementary material document. This figure shows representative extracted ion chromatograms of the uncyclized brGDGTs (Ia, IIa, IIIa and their isomers) and OB-GDGT$_{1064}$ and its isomers. Supplementary material to this article can be found online at https://doi.org/10.1016/j.gca.2024.01.034.

References

Anderson, V.J., Shanahan, T.M., Saylor, J.E., Horton, B.K., Mora, A.R., 2014. Sources of local and regional variability in the MBT′/CBT paleotemperature proxy: insights from a modern elevation transect across the Eastern Cordillera of Colombia. Org. Geochem. 69, 42–51.

Bligh, E.G., Dyer, W.J., 1959. A rapid method of total lipid extraction and purification. Can. J. Biochem. Physiol. 37, 911–917.

Chen, Y., Zheng, F., Yang, H., Yang, W., Wu, R., Liu, X., Liang, H., Chen, H., Pei, H., Zhang, C., Pancost, R.D., Zeng, Z., 2022. The production of diverse brGDGTs by an Acidobacterium providing a physiological basis for paleoclimate proxies. Geochim. Cosmochim. Acta 337, 155–165.

Dang, X., Yang, H., Naafs, B.D.A., Pancost, R.D., Xie, S., 2016. Evidence of moisture control on the methylation of branched glycerol dialkyl glycerol tetraethers in semi-arid and arid soils. Geochim. Cosmochim. Acta 189, 24–36.

De Jonge, C., Hopmans, E.C., Stadnitskaia, A., Rijpstra, W.I.C., Hofland, R., Tegelaar, E., Damsté, J.S.S., 2013. Identification of novel penta- and hexamethylated branched glycerol dialkyl glycerol tetraethers in peat using HPLC-MS2, GC-MS and GC-SMB-MS. Org. Geochem. 54, 78–82.

De Jonge, C., Hopmans, E.C., Zell, C.I., Kim, J.H., Schouten, S., Damsté, J.S.S., 2014. Occurrence and abundance of 6-methyl branched glycerol dialkyl glycerol tetraethers in soils: Implications for palaeoclimate reconstruction. Geochim. Cosmochim. Acta 141, 97–112.

De Jonge, C., Radujković, D., Sigurdsson, B.D., Weedon, J.T., Janssens, I., Peterse, F., 2019. Lipid biomarker temperature proxy responds to abrupt shift in the bacterial community composition in geothermally heated soils. Org. Geochem. 137.

Dearing Crampton-Flood, E., Tierney, J.E., Peterse, F., Kirkels, F.M.S.A., Damsté, J.S.S., 2020. BayMBT: a Bayesian calibration model for branched glycerol dialkyl glycerol tetraethers in soils and peats. Geochim. Cosmochim. Acta 268, 142–159.

Dillon, J.T., Lash, S., Zhao, J., Smith, K.P., van Dommelen, P., Scherer, A.K., Huang, Y., 2018. Bacterial tetraether lipids in ancient bones record past climate conditions at the time of disposal. J. Archaeol. Sci. 96, 45–56.

Ding, S., Schwab, V.F., Ueberschaar, N., Roth, V.-N., Lange, M., Xu, Y., Gleixner, G., Pohnert, G., 2016. Identification of novel 7-methyl and cyclopentanyl branched glycerol dialkyl glycerol tetraethers in lake sediments. Org. Geochem. 102, 52–58.

Drotz, S.H., Sparrman, T., Nilsson, M.B., Schleucher, J., Öquist, M.G., 2010. Both catabolic and anabolic heterotrophic microbial activity proceed in frozen soils. Proc. Natl. Acad. Sci. U. S. A. 107, 21046–21051.

Dugerdil, L., Joannin, S., Peyron, O., Jouffroy-Bapicot, I., Vannière, B., Boldgiv, B., Unkelbach, J., Behling, H., Ménot, G., 2021. Climate reconstructions based on GDGT and pollen surface datasets from Mongolia and Baikal area: Calibrations and applicability to extremely cold-dry environments over the Late Holocene. Clim. past 17, 1199–1226.

Evans, S.G., Raberg, J.H., Crump, S.E., Raynolds, M.K., Sugg, M.M., Brodie, A.R., Miller, G.H., 2022. Control of short-stature vegetation type on shallow ground temperatures in permafrost across the eastern Canadian Arctic. J. Geophys. Res. – Biogeosci. 1–16.

Fuchs, L., Zhou, B., Magill, C., Eglinton, T.I., Sun, Y., Peterse, F., 2022. Multiproxy records of temperature, precipitation and vegetation on the central Chinese Loess Plateau over the past 200,000 years. Quat. Sci. Rev. 288, 107579.

Halamka, T.A., Raberg, J.H., McFarlin, J.M., Younkin, A.D., Mulligan, C., Liu, X.-L., Kopf, S.H., Toby, H.C.A., 2022. Production of diverse brGDGTs by Acidobacterium Solibacter usitatus in response to temperature, pH, and O_2 provides a culturing perspective on brGDGT proxies and biosynthesis. Geobiology 00, 1–17.

Halffman, R., Lembrechts, J., Radujković, D., De Gruyter, J., Nijs, I., De Jonge, C., 2022. Soil chemistry, temperature and bacterial community composition drive brGDGT distributions along a subarctic elevation gradient. Org. Geochem. 163, 104346.

Heijmans, M.M.P.D., Magnússon, R., Lara, M.J., Frost, G.V., Myers-Smith, I.H., van Huissteden, J., Jorgenson, M.T., Fedorov, A.N., Epstein, H.E., Lawrence, D.M., Limpens, J., 2022. Tundra vegetation change and impacts on permafrost. Nat. Rev. Earth Environ. 3, 68–84.

Hopmans, E.C., Schouten, S., Sinninghe, J.S., 2016. The effect of improved chromatography on GDGT-based palaeoproxies. Org. Geochem. 93, 1–6.

Huguet, C., Hopmans, E.C., Febo-Ayala, W., Thompson, D.H., Sinninghe, D.J.S., Schouten, S., 2006. An improved method to determine the absolute abundance of glycerol dibiphytanyl glycerol tetraether lipids. Org. Geochem. 37, 1036–1041.

Huguet, A., Meador, T.B., Laggoun-Défarge, F., Könneke, M., Wu, W., Derenne, S., Hinrichs, K.-U., 2017. Production rates of bacterial tetraether lipids and fatty acids in peatland under varying oxygen concentrations. Geochim. Cosmochim. Acta 203, 103–116.

Inglis, G.N., Bhattacharya, T., Hemingway, J.D., Hollingsworth, E.H., Feakins, S.J., Tierney, J.E., 2022. Biomarker approaches for reconstructing terrestrial environmental change. Annu. Rev. Earth Planet. Sci. 50, 369–394.

IPCC, 2022. *IPCC, 2022: Climate Change 2022: Impacts, Adaptation, and Vulnerability. Contribution of Working Group II to the Sixth Assessment Report of the Intergovernmental Panel on Climate Change*. Pörtner, H.O., Roberts, D.C., Tignor, M., Poloczanska, E.S., Mintenbeck, K., Alegría, A., Craig, M., Langsdorf, S., Löschke, S., Möller, V., Okem, A., Rama, B. (Eds.) Cambridge University Press.

Kemp, D.B., Robinson, S.A., Crame, J.A., Francis, J.E., Ineson, J., Whittle, R.J., Bowman, V., O'Brien, C., 2014. A cool temperate climate on the Antarctic Peninsula through the latest Cretaceous to early Paleogene. Geology 42, 583–586.

Komsta, L., Novomestky, F., 2022. moments: Moments, Cumulants, Skewness, Kurtosis and Related Tests.

Kou, Q., Zhu, L., Ju, J., Wang, J., Xu, T., Li, C., Ma, Q., 2022. Influence of salinity on glycerol dialkyl glycerol tetraether-based indicators in Tibetan Plateau lakes: implications for paleotemperature and paleosalinity reconstructions. Palaeogeogr. Palaeoclimatol. Palaeoecol. 601, 111127.

Kropp, H., Loranty, M.M., Natali, S.M., Kholodov, A.L., Rocha, A.V., Myers-Smith, I., Abbot, B.W., Abermann, J., Blanc-Betes, E., Blok, D., Blume-Werry, G., Boike, J., Breen, A.L., Cahoon, S.M.P., Christiansen, C.T., Douglas, T.A., Epstein, H.E., Frost, G. V., Goeckede, M., Hoye, T.T., Mamet, S.D., O'Donnell, J.A., Olefeldt, D., Phoenix, G. K., Salmon, V.G., Sannel, A.B.K., Smith, S.L., Sonnentag, O., Vaughn, L.S., Williams, M., Elberling, B., Gough, L., Hjort, J., Lafleur, P.M., Euskirchen, E.S., Heijmans, M.M.P.D., Humphreys, E.R., Iwata, H., Jones, B.M., Jorgenson, M.T., Grünberg, I., Kim, Y., Laundre, J., Mauritz, M., Michelsen, A., Schaepman-Strub, G., Tape, K.D., Ueyama, M., Lee, B.Y., Langley, K., Lund, M., 2021. Shallow soils are warmer under trees and tall shrubs across Arctic and Boreal ecosystems. Environ. Res. Lett. 16, 015001.

Kwiecien, O., Braun, T., Brunello, C.F., Faulkner, P., Hausmann, N., Helle, G., Hoggarth, J.A., Ionita, M., Jazwa, C.S., Kelmelis, S., Marwan, N., Nava-Fernandez, C., Nehme, C., Opel, T., Oster, J.L., Perşoiu, A., Petrie, C., Prufer, K., Saarni, S.M., Wolf, A., Breitenbach, S.F.M., 2022. What we talk about when we talk about seasonality – A transdisciplinary review. Earth-Science Rev. 225, 103843.

Lembrechts, J.J., Aalto, J., Ashcroft, M.B., De Frenne, P., Kopecký, M., Lenoir, J., Luoto, M., Maclean, I.M.D., Roupsard, O., Fuentes-Lillo, E., García, R.A., Pellissier, L., Pitteloud, C., Alatalo, J.M., Smith, S.W., Björk, R.G., Muffler, L., Ratier, B.A., Cesarz, S., Gottschall, F., Okello, J., Urban, J., Plichta, R., Svátek, M., Phartyal, S.S., Wipf, S., Eisenhauer, N., Puşcaş, M., Turtureanu, P.D., Varlagin, A., Dimarco, R.D., Jump, A.S., Randall, K., Dorrepaal, E., Larson, K., Walz, J., Vitale, L., Svoboda, M., Finger, H.R., Halbritter, A.H., Curasi, S.R., Klupar, I., Koontz, A., Pearse, W.D., Simpson, E., Stemkovski, M., Jessen, G.B., Vedel, S.M., Høye, T.T., Fernández, C.M.R., Lorite, J., Carbognani, M., Tomaselli, M., Forte, T.G.W.,

Petraglia, A., Haesen, S., Somers, B., Van Meerbeek, K., Björkman, M.P., Hylander, K., Merinero, S., Gharun, M., Buchmann, N., Dolezal, J., Matula, R., Thomas, A.D., Bailey, J.J., Ghosn, D., Kazakis, G., de Pablo, M.A., Kemppinen, J., Niittynen, P., Rew, L., Seipel, T., Larson, C., Speed, J.D.M., Ardö, J., Cannone, N., Guglielmin, M., Malfasi, F., Bader, M.Y., Canessa, R., Stanisci, A., Kreyling, J., Schmeddes, J., Teuber, L., Aschero, V., Čiliak, M., Máliš, F., De Smedt, P., Govaert, S., Meeussen, C., Vangansbeke, P., Gigauri, K., Lamprecht, A., Pauli, H., Steinbauer, K., Winkler, M., Ueyama, M., Nuñez, M.A., Ursu, T.M., Haider, S., Wedegärtner, R.E.M., Smiljanic, M., Trouillier, M., Wilmking, M., Altman, J., Brůna, J., Hederová, L., Macek, M., Man, M., Wild, J., Vittoz, P., Pärtel, M., Barančok, P., Kanka, R., Kollár, J., Palaj, A., Barros, A., Mazzolari, A.C., Bauters, M., Boeckx, P., Benito, A.J.L., Zong, S., Di Cecco, V., Sitková, Z., Tielbörger, K., van den Brink, L., Weigel, R., Homeier, J., Dahlberg, C.J., Medinets, S., Medinets, V., De Boeck, H.J., Portillo-Estrada, M., Verryckt, L.T., Milbau, A., Daskalova, G.N., Thomas, H.J.D., Myers-Smith, I.H., Blonder, B., Stephan, J.G., Descombes, P., Zellweger, F., Frei, E.R., Heinesch, B., Andrews, C., Dick, J., Siebicke, L., Rocha, A., Senior, R.A., Rixen, C., Jimenez, J.J., Boike, J., Pauchard, A., Scholten, T., Scheffers, B., Klinges, D., Basham, E.W., Zhang, J., Zhang, Z., Géron, C., Fazlioglu, F., Candan, O., Sallo, B.J., Hrbacek, F., Laska, K., Cremonese, E., Haase, P., Moyano, F. E., Rossi, C., Nijs, I., 2020. SoilTemp: A global database of near-surface temperature. Glob. Chang. Biol. 26, 6616–6629.

Liang, J., Russell, J.M., Xie, H., Lupien, R.L., Si, G., Wang, J., Hou, J., Zhang, G., 2019. Vegetation effects on temperature calibrations of branched glycerol dialkyl glycerol tetraether (brGDGTs) in soils. Org. Geochem. 127, 1–11.

Liu, X.L., Summons, R.E., Hinrichs, K.U., 2012. Extending the known range of glycerol ether lipids in the environment: Structural assignments based on tandem mass spectral fragmentation patterns. Rapid Commun. Mass Spectrom. 26, 2295–2302.

Liu, X.L., Zhu, C., Wakeham, S.G., Hinrichs, K.U., 2014. In situ production of branched glycerol dialkyl glycerol tetraethers in anoxic marine water columns. Mar. Chem. 166, 1–8.

Loranty, M.M., Abbott, B.W., Blok, D., Douglas, T.A., Epstein, H.E., Forbes, B.C., Jones, B. M., Kholodov, A.L., Kropp, H., Malhotra, A., Mamet, S.D., Myers-Smith, I.H., Natali, S.M., O'Donnell, J.A., Phoenix, G.K., Rocha, A.V., Sonnentag, O., Tape, K.D., Walker, D.A., 2018. Reviews and syntheses: Changing ecosystem influences on soil thermal regimes in northern high-latitude permafrost regions. Biogeosciences 15, 5287–5313.

Lu, H., Liu, W., Wang, H., Wang, Z., 2016. Variation in 6-methyl branched glycerol dialkyl glycerol tetraethers in Lantian loess–paleosol sequence and effect on paleotemperature reconstruction. Org. Geochem. 100, 10–17.

Lu, H., Liu, W., Yang, H., Wang, H., Liu, Z., Leng, Q., Sun, Y., Zhou, W., An, Z., 2019. 800-kyr land temperature variations modulated by vegetation changes on Chinese Loess Plateau. Nat. Commun. 10.

Lü, X., Liu, X., Xu, C., Song, J., Li, X., Huamao, Y., Li, N., Wang, D., Hongming, Y., Ye, S., 2019. The origins and implications of glycerol ether lipids in China coastal wetland sediments. Sci. Rep. 9, 18529.

Lu, H., Liu, W., Yang, H., Leng, Q., Liu, Z., Cao, Y., Hu, J., Sheng, W., Wang, H., Wang, Z., Zhang, Z., Sun, Y., Zhou, W., An, Z., 2022. Decoupled Land and Ocean Temperature Trends in the Early-Middle Pleistocene. Geophys. Res. Lett. 49, 1–9.

Lumley, T., 2020. leaps: Regression Subset Selection.

Martin, C., Ménot, G., Thouveny, N., Davtian, N., Andrieu-Ponel, V., Reille, M., Bard, E., 2019. Impact of human activities and vegetation changes on the tetraether sources in Lake St Front (Massif Central, France). Org. Geochem. 135, 38–52.

Martínez-Sosa, P., Tierney, J.E., Stefanescu, I.C., Dearing, C.-F., Shuman, B.N., Routson, C., 2021. A global Bayesian temperature calibration for lacustrine brGDGTs. Geochim. Cosmochim. Acta 305, 87–105.

McMahon, S.K., Wallenstein, M.D., Schimel, J.P., 2009. Microbial growth in Arctic tundra soil at −2°C. Environ. Microbiol. Rep. 1, 162–166.

Molnar, P., 2022. Differences between soil and air temperatures: Implications for geological reconstructions of past climate. Geosphere 18.

Naafs, B.D.A., Gallego-Sala, A.V., Inglis, G.N., Pancost, R.D., 2017. Refining the global branched glycerol dialkyl glycerol tetraether (brGDGT) soil temperature calibration. Org. Geochem. 106, 48–56.

Naafs, B.D.A., Oliveira, A.S.F., Mulholland, A.J., 2021. Molecular dynamics simulations support the hypothesis that the brGDGT paleothermometer is based on homeoviscous adaptation. Geochim. Cosmochim Acta.

Nieto-Moreno, V., Rohrmann, A., van der Meer, M.T.J., Sinninghe, D.J.S., Sachse, D., Tofelde, S., Niedermeyer, E.M., Strecker, M.R., Mulch, A., 2016. Elevation-dependent changes in n-alkane δD and soil GDGTs across the South Central Andes. Earth Planet. Sci. Lett. 453, 234–242.

Öquist, M.G., Sparrman, T., Klemedtsson, L., Drotz, S.H., Grip, H., Schleucher, J., Nilsson, M.S., 2009. Water availability controls microbial temperature responses in frozen soil CO_2 production. Glob. Chang. Biol. 15, 2715–2722.

Pancost, R.D., Taylor, K.W.R., Inglis, G.N., Kennedy, E.M., Handley, L., Hollis, C.J., Crouch, E.M., Pross, J., Huber, M., Schouten, S., Pearson, P.N., Morgans, H.E.G., Raine, J.I., 2013. Early Paleogene evolution of terrestrial climate in the SW Pacific, Southern New Zealand. Geochem. Geophys. Geosyst. 14, 5413–5429.

Panikov, N.S., 2005. Contribution of nanosized bacteria to the total biomass and activity of a soil microbial community. Adv. Appl. Microbiol. 57, 245–296.

Panikov, N.S., Flanagan, P.W., Oechel, W.C., Mastepanov, M.A., Christensen, T.R., 2006. Microbial activity in soils frozen to below −39 °C. Soil Biol. Biochem. 38, 785–794.

Pérez-Angel, L.C., Sepúlveda, J., Molnar, P., Montes, C., Rajagopalan, B., Snell, K., Gonzalez-Arango, C., Dildar, N., 2020. Soil and air temperature calibrations using branched GDGTs for the tropical andes of Colombia: toward a pan-tropical calibration. Geochem. Geophys. Geosyst. 21, 1–18.

Peterse, F., Nicol, G.W., Schouten, S., Damsté, J.S.S., 2010. Influence of soil pH on the abundance and distribution of core and intact polar lipid-derived branched GDGTs in soil. Org. Geochem. 41, 1171–1175.

Peterse, F., Meer, J., Der, V., Schouten, S., Weijers, J.W.H.H., Fierer, N., Jackson, R.B., Kim, J.H., Damste, J.S.S., 2012. Revised calibration of the MBT – CBT paleotemperature proxy based on branched tetraether membrane lipids in surface soils. Geochim. Cosmochim. Acta 96, 215–229.

Peterse, F., Martínez-García, A., Zhou, B., Beets, C.J., Prins, M.A., Zheng, H., Eglinton, T. I., 2014. Molecular records of continental air temperature and monsoon precipitation variability in East Asia spanning the past 130,000 years. Quat. Sci. Rev. 83, 76–82.

Raberg, J.H., Harning, D.J., Crump, S.E., De Wet, G., Blumm, A., Kopf, S., Geirsdóttir, Á., Miller, G.H., Sepúlveda, J., 2021a. Revised fractional abundances and warm-season temperatures substantially improve brGDGT calibrations in lake sediments. Biogeosciences 18, 3579–3603.

Raberg, J.H., Harning, D.J., Geirsdóttir, Á., Sepúlveda, J., Miller, G.H., 2021b. Soil and lake water temperatures of Iceland (2019–2021). Arct. Data Cent.

Raberg, J.H., Flores, E., Crump, S.E., de Wet, G., Dildar, N., Miller, G.H., Geirsdóttir, Á., Sepúlveda, J., 2022a. Intact Polar brGDGTs in Arctic Lake catchments: implications for lipid sources and paleoclimate applications. J. Geophys. Res. Biogeosci. 127, e2022JG006969.

Raberg, J.H., Miller, G.H., Geirsdóttir, Á., Sepúlveda, J., 2022b. Near-universal trends in brGDGT lipid distributions in nature. Sci. Adv. 8, 7625.

Raberg, J.H., de Wet, G., Crump, S.E., Raynolds, M.K., Sepúlveda, J., Miller, G.H., 2022c. Air, soil, and lake water temperatures of the Eastern Canadian Arctic (2017–2021). Arct. Data Cent.

Rodrigo-Gámiz, M., García-Alix, A., Jiménez-Moreno, G., Ramos-Román, M.J., Camuera, J., Toney, J.L., Sachse, D., Anderson, R.S., Damsté, J.S.S., 2022. Paleoclimate reconstruction of the last 36 kyr based on branched glycerol dialkyl glycerol tetraethers in the Padul palaeolake record (Sierra Nevada, southern Iberian Peninsula). Quat. Sci. Rev. 281, 107434.

Romanovsky, V.E., Osterkamp, T.E., 2000. Effects of unfrozen water on heat and mass transport processes in the active layer and permafrost. Permafr. Periglac. Process. 11, 219–239.

Rueda, G., Rosell-Melé, A., Escala, M., Gyllencreutz, R., Backman, J., 2009. Comparison of instrumental and GDGT-based estimates of sea surface and air temperatures from the Skagerrak. Org. Geochem. 40, 287–291.

Sachs, J.P., Pahnke, K., Smittenberg, R., Zhang, Z., 2013. Biomarker Indicators of Past Climate. In: Encyclopedia of Quaternary Science, 2nd edn., pp. 775–782.

Schreuder, L.T., Beets, C.J., Prins, M.A., Hatté, C., Peterse, F., 2016. Late Pleistocene climate evolution in Southeastern Europe recorded by soil bacterial membrane lipids in Serbian loess. Palaeogeogr. Palaeoclimatol. Palaeoecol. 449, 141–148.

Schwarz, G., 1978. Estimating the Dimension of a Model. Ann. Stat. 6, 461–464.

Segura, J.H., Nilsson, M.B., Schleucher, J., Haei, M., Sparrman, T., Székely, A., Bertilsson, S., Öquist, M.G., 2019. Microbial utilization of simple carbon substrates in boreal peat soils at low temperatures. Soil Biol. Biochem. 135, 438–448.

Sigurdsson, B.D., Leblans, N.I.W., Dauwe, S., Gudmundsdóttir, E., Gundersen, P., Gunnarsdóttir, G.E., Holmstrup, M., Ilieva-Makulec, K., Kätterer, T., Marteinsdóttir, B., Maljanen, M., Oddsdóttir, E.S., Ostonen, I., Peñuelas, J., Poeplau, C., Richter, A., Sigurdsson, P., Van Bodegom, P., Wallander, H., Weedon, J., Janssens, I., 2016. Geothermal ecosystems as natural climate change experiments: The ForHot research site in Iceland as a case study. Icelandic Agric. Sci. 29, 53–71.

Slessarev, E.W., Lin, Y., Bingham, N.L., Johnson, J.E., Dai, Y., Schimel, J.P., Chadwick, O. A., 2016. (2016) Water balance creates a threshold in soil pH at the global scale. Nat. 5407634 (540), 567–569.

Sparrman, T., Öquist, M., Klemedtsson, L., Schleucher, J., Nilsson, M., 2004. Quantifying unfrozen water in frozen soil by high-field 2H NMR. Environ. Sci. Technol. 38, 5420–5425.

Steven, B., Pollard, W.H., Greer, C.W., Whyte, L.G., 2008. Microbial diversity and activity through a permafrost/ground ice core profile from the Canadian high Arctic. Environ. Microbiol. 10, 3388–3403.

Sun, W., Zhao, S., Pei, H., Yang, H., 2019. The coupled evolution of mid- to late Holocene temperature and moisture in the southeast Qaidam Basin. Chem. Geol. 528, 119282.

Super, J.R., Chin, K., Pagani, M., Li, H., Tabor, C., Harwood, D.M., Hull, P.M., 2018. Late Cretaceous climate in the Canadian Arctic: Multi-proxy constraints from Devon Island. Palaeogeogr. Palaeoclimatol. Palaeoecol. 504, 1–22.

Team R Development Core, 2021. R: A language and environment for statistical computing. R Found. Stat. Comput. 2.

Tibbett, E.J., Warny, S., Tierney, J.E., Wellner, J.S., Feakins, S.J., 2022. Cenozoic Antarctic Peninsula temperatures and glacial erosion signals from a multi-proxy biomarker study. Paleoceanogr. Paleoclimatology 37 e2022PA004430.

Tierney, J.E., Russell, J.M., Eggermont, H., Hopmans, E.C., Verschuren, D., Damsté, J.S. S., 2010. Environmental controls on branched tetraether lipid distributions in tropical East African lake sediments. Geochim. Cosmochim. Acta 74, 4902–4918.

Tierney, J.E., Poulsen, C.J., Montañez, I.P., Bhattacharya, T., Feng, R., Ford, H.L., Hönisch, B., Inglis, G.N., Petersen, S.V., Sagoo, N., Tabor, C.R., Thirumalai, K., Zhu, J., Burls, N.J., Foster, G.L., Goddéris, Y., Huber, B.T., Ivany, L.C., Turner, S.K., Lunt, D.J., McElwain, J.C., Mills, B.J.W., Otto-Bliesner, B.L., Ridgwell, A., Zhang, Y. G., 2020. Past climates inform our future. Science 80-, 370.

Torrance, J.K., Schellekens, F.J., 2006. Chemical factors in soil freezing and frost heave. Polar Rec. (gr. Brit) 42, 33–42.

Tuorto, S.J., Darias, P., McGuinness, L.R., Panikov, N., Zhang, T., Häggblom, M.M., Kerkhof, L.J., 2014. (2013) Bacterial genome replication at subzero temperatures in permafrost. ISME J. 81 (8), 139–149.

Venables, W.N., Ripley, B.D., 2002. Modern Applied Statistics with S, fourth edn. Springer, New York.

Véquaud, P., Thibault, A., Derenne, S., Anquetil, C., Collin, S., Contreras, S., Nottingham, A.T., Sabatier, P., Werne, J.P., Huguet, A., 2022. FROG: a global machine-learning temperature calibration for branched GDGTs in soils and peats. Geochim. Cosmochim. Acta 318, 468–494.

von Oppen, J., Assmann, J.J., Bjorkman, A.D., Treier, U.A., Elberling, B., Nabe-Nielsen, J., Normand, S., 2022. Cross-scale regulation of seasonal microclimate by vegetation and snow in the Arctic tundra. Glob. Chang. Biol. 28, 7296–7312.

Wang, H., An, Z., Lu, H., Zhao, Z., Liu, W., 2020. Calibrating bacterial tetraether distributions towards in situ soil temperature and application to a loess-paleosol sequence. Quat. Sci. Rev. 231, 106172.

Wang, H., Liu, W., 2021. Soil temperature and brGDGTs along an elevation gradient on the northeastern Tibetan Plateau: A test of soil brGDGTs as a proxy for paleoelevation. Chem. Geol. 566, 120079.

Wang, H., Liu, W., Lu, H., 2016. Appraisal of branched glycerol dialkyl glycerol tetraether-based indices for North China. Org. Geochem. 98, 118–130.

Wang, H., Liu, W., He, Y., Zhou, A., Zhao, H., Liu, H., Cao, Y., Hu, J., Meng, B., Jiang, J., Kolpakova, M., Krivonogov, S., Liu, Z., 2021. Salinity-controlled isomerization of lacustrine brGDGTs impacts the associated MBT5ME' terrestrial temperature index. Geochim. Cosmochim. Acta 305, 33–48.

Weber, Y., De Jonge, C., Rijpstra, W.I.C., Hopmans, E.C., Stadnitskaia, A., Schubert, C.J., Lehmann, M.F., Sinninghe, D.J.S., Niemann, H., 2015. Identification and carbon isotope composition of a novel branched GDGT isomer in lake sediments: Evidence for lacustrine branched GDGT production. Geochim. Cosmochim. Acta 154, 118–129.

Weber, Y., Damsté, J.S.S., Zopfi, J., De Jonge, C., Gilli, A., Schubert, C.J., Lepori, F., Lehmann, M.F., Niemann, H., 2018. Redox-dependent niche differentiation provides evidence for multiple bacterial sources of glycerol tetraether lipids in lakes. Proc. Natl. Acad. Sci. u. s. a. 115, 10926–10931.

Weijers, J.W.H., Schouten, S., Hopmans, E.C., Geenevasen, J.A.J., David, O.R.P., Coleman, J.M., Pancost, R.D., Damsté, J.S.S., 2006. Membrane lipids of mesophilic anaerobic bacteria thriving in peats have typical archaeal traits. Environ. Microbiol. 8, 648–657.

Weijers, J.W.H., Schefuß, E., Schouten, S., Damsté, J.S.S., 2007a. Coupled thermal and hydrological evolution of tropical Africa over the last deglaciation. Science (80-.) 315, 1701–1704.

Weijers, J.W.H., Schouten, S., Donker, J.C., Den, V., Hopmans, E.C., van den Donker, J. C., Hopmans, E.C., Damsté, J.S.S., 2007b. Environmental controls on bacterial tetraether membrane lipid distribution in soils. Geochim. Cosmochim. Acta 71, 703–713.

Weijers, J.W.H., Schouten, S., Sluijs, A., Brinkhuis, H., Damsté, J.S.S., 2007c. Warm arctic continents during the Palaeocene-Eocene thermal maximum. Earth Planet. Sci. Lett. 261, 230–238.

Weijers, J.W.H., Wiesenberg, G.L.B., Bol, R., Hopmans, E.C., Pancost, R.D., 2010. Carbon isotopic composition of branched tetraether membrane lipids in soils suggest a rapid turnover and a heterotrophic life style of their source organism(s). Biogeosciences 7, 2959–2973.

Weijers, J.W.H., Bernhardt, B., Peterse, F., Werne, J.P., Dungait, J.A.J., Schouten, S., Damsté, J.S.S., 2011. Absence of seasonal patterns in MBT-CBT indices in mid-latitude soils. Geochim. Cosmochim. Acta 75, 3179–3190.

Wörmer, L., Lipp, J.S., Schröder, J.M., Hinrichs, K.U., 2013. Application of two new LC-ESI-MS methods for improved detection of intact polar lipids (IPLs) in environmental samples. Org. Geochem. 59, 10–21.

Xiao, W., Xu, Y., Ding, S., Wang, Y., Zhang, X., Yang, H., Wang, G., Hou, J., 2015. Global calibration of a novel, branched GDGT-based soil pH proxy. Org. Geochem. 89–90, 56–60.

Xie, S., Liu, X.L., Schubotz, F., Wakeham, S.G., Hinrichs, K.U., 2014. Distribution of glycerol ether lipids in the oxygen minimum zone of the Eastern Tropical North Pacific Ocean. Org. Geochem. 71, 60–71.

Youfeng, N., Weiguo, L., Zhisheng, A., 2008. A 130-ka reconstruction of precipitation on the Chinese Loess Plateau from organic carbon isotopes. Palaeogeogr. Palaeoclimatol. Palaeoecol. 270, 59–63.

Yu, J., Sun, W., Liu, J., Wang, J., Yang, J., Meixner, F.X., 2007. Enhanced net formations of nitrous oxide and methane underneath the frozen soil in Sanjiang wetland, northeastern China. J. Geophys. Res. Atmos. 112, 2–9.

Zang, J., Lei, Y., Yang, H., 2018. Distribution of glycerol ethers in Turpan soils: implications for use of GDGT-based proxies in hot and dry regions. Front. Earth Sci. 12, 862–876.

Zeng, F., Yang, H., 2019. Temperature changes reconstructed from branched GDGTs on the central Loess Plateau during the past 130–5 ka. Quat. Int. 503, 3–9.

Zhang, T., 2005. Influence of the seasonal snow cover on the ground thermal regime: an overview. Rev. Geophys. 43, 4002.

Zhao, J., Huang, Y., Yao, Y., An, Z., Zhu, Y., Lu, H., Wang, Z., 2020. Calibrating branched GDGTs in bones to temperature and precipitation: application to Alaska chronological sequences. Quat. Sci. Rev. 240, 106371.

Zhao, J., Tsai, V.C., Huang, Y., 2022. A nonlinear model for resolving the temperature bias of branched glycerol dialkyl glycerol tetraether (brGDGT) temperature proxies. Geochim. Cosmochim. Acta 327, 158–169.

Zheng, Y., Liu, H., Yang, H., Wang, H., Zhao, W., Zhang, Z., Huang, M., Liu, W., 2022. Decoupled Asian monsoon intensity and precipitation during glacial-interglacial transitions on the Chinese Loess Plateau. Nat. Commun. 13, 1–13.